공학박사 학위논문

Nanocellulose Embedded Polymer Composite Foams for Flame Retardancy

난연성 향상을 위한 나노셀룰로오스 충진 고분자 복합재료 폼

2019년 8월

서울대학교 대학원

재료공학부

김 한 수

Nanocellulose Embedded Polymer Composite Foams for Flame Retardancy

난연성 향상을 위한 나노셀룰로오스 충진 고분자 복합재료 폼

지도 교수 윤 재 륜

이 논문을 공학박사 학위논문으로 제출함
2019 년 7 월

서울대학교 대학원
재료공학부
김 한 수

김한수의 박사 학위논문을 인준함
2019 년 6 월

위 원 장 안 철 희 (인)

부위원장 윤 재 륜 (인)

위 원 유 웅 열 (인)

위 원 정 준 호 (인)

위 원 송 영 석 (인)

Doctoral Dissertation in Engineering

Nanocellulose Embedded Polymer Composite Foams for Flame Retardancy

by

Hansu Kim

Advisor: Prof. Jae Ryoun Youn

August 2019

Department of Materials Science and Engineering

Graduate School

Seoul National University

Abstract

Chapter I explains an overview of nanocellulose and flame retardant properties. Nanocelluloses are used in various applications to improve the quilty of human life. Although nanocelluloses are venerable to fire, these properies can be modifired by chemical treatement such as silylation. This can be used to flame retradanct materials itself and used to flame retradant filler with polymeric composites.

Chapter II provides an fabrication of silylated Nanocrystalline cellulose (NCC) for flame retardant application. Employing proper flame retardant materials is one of the most important fire safety guidelines when constructing buildings. Most flame retardants, however, contain halogen atoms that might become harmful gases to human body during combustion. We designed and fabricated an environmental-friendly flame retardant material with a superior performance for thermal insulation. NCC was prepared using acid hydrolysis method, and its surface was chemically modified through silylation treatment. Various characteristics of the flame retardant material, such as morphology, chemical structure, thermal stability, and thermal conductivity were investigated. When a mass ratio of NCC to methyltrimethoxysilane (MTMS) was 1:5, the limiting oxygen index (LOI) of the silylated NCC increased to 34% and a char yield of 80% was obtained. The silylation led to enhancement in the thermal stability of NCC and generation of the char residue. Chemical structure of the residual materials after combustion was investigated by using Fourier transform infrared spectroscopy (FTIR) and X-ray differential photo spectroscopy (XPS).

Chapter III demonstrates fabrication of silylated nanofibrillated cellulose and polyurethane composite with TCPP. Improving flame retardancy is one of the most crucial issues to use polymeric materials for building construction. Most of the flame retardant materials containing halogen atoms delay fire spread, but produce harmful gases during combustion. Hence, we designed and fabricated a composite foam by using a green nanomaterial. Silylated and nanofibrillated cellulose (Si-NFC) was added to polyurethane foam (PUF) containing tris(2-chloropropyl) phosphate (TCPP) in order to reduce the emission of smoke during combustion. Thermal characteristics of the composite foams were investigated through thermogravimetric analysis, LOI, and cone

calorimeter tests. The LOI of the Si-NFC embedded composite was increased from 19.3% to 24.6%. In addition, the Si-NFC led to an improvement in the thermal stability of the composites by reducing the peak release of heat and smoke. Chemical structure of the residual char was analyzed by using energy-dispersive X-ray spectroscopy and Fourier transform infrared spectroscopy.

In Chapter IV, the increment of flame retardant propterties of polyurthane composite with TCEP are explained. Delaying flame propagation in the event of a fire can increase the likelihood of preserving life and alleviate damage to property. Here, a strategy for flame retardant polymer composite foam is proposed, which enables the improved performance, good formability, and reduced environmental burden while burning. The strategy is to incorporate sylilated nanocellulose into a polyurethane matrix containing a conventional flame retardant, Tris(2-chloroethyl) phosphate (TCEP). This strategy leads to the generation of char layer faster during combustion, resulting in a delayed flame propagation. The LOI of the samples increased by 28%, and the production rate of toxic gas emission was considerably reduced. The chemical, thermomechanical, and morphological analyses were carried out to understand the underlying physics.

Keywords: Polymeric material, Nanocellulose, nanocrystalline cellulose, nanofibrillated cellulose, silylation, silylated cellulose, flame retardancy, polyurethane foam, composite, composite foam.

Student Number: 2014-30203

Contents

List of Figures

List of Tables

Chapter I.

Introduction

1.1. What is a nanocellulose?

1.1.1. The types of nanocellulose

Cellulose is a linear chain polymer in the natural polysaccharides based on glucose, one of the most abundant natural polymers on the planet.[1,2] It is not only a sustainable material, but also an environmentally degradable material that can be decomposed. When cellulose has a nanostructure, its crystallinity, strength, physical chemical, and thermal properties are improved. The properties of nanocellulose depend on the raw material and manufacturing method (see **Figure 1.1.1**).

Firstly, nanocrystalline cellulose (NCC) can be fabricated by acid treatment or ultrasonic method due to its crystalline region and amorphous region.[3,4] When acid or ultrasonic wave is applied to microcrystalline cellulose (MCC) from a wood, the relative weak amorphous part is decomposed and converted to a glucose, leaving only the crystalline part with high strength. Since its structure is needle-like shaped, it is also called a nanowhisker. It can be used as a filler to improve mechanical strength of polymeric composite. The drawback of this method is that a large amount of sulfuric acid is used or decomposed a lot of cellulose to form a NCC.

Secondly, microfibrillated cellulose (MFC) can be prepared from the bleached Kraft pulp. Based on this cellulose, nanofibrillated cellulose (NFC) can be prepared from the microfibrillated cellulose (MFC) using a microfluidizer.[5] For the purpose of more fibrillated cellulose, 2,2,6,6-Tetramethyl-1-piperidinyloxy (TEMPO) oxidation can be employed to obtain nano-sized diameter of NFC.[6] The benefit of this cellulose is that it has high aspect ratio, absorbs water well, and has no crystalline structure. It also has good biocompatibility, but it consumes lots of energy in the fibrillation process.

Finally, a nanocellulose can be cultivated from several bacteria species. The advantage of bacterial cellulose is that it consists of a pure cellulose structure without a hemicellulose and lignin.[7,8] It has high strength, crystalline structures, and high aspect ratio, but it is difficult to mass-produce.

Additionally, a cellulose can be classified by a solubility. α-cellulse has insiluble in 17.5 wt% sodium hydroxide soulution. From the supernatant, the mixture of β-cellulose and γ-cellulose are exsisted. β-cellulose is precipitated solid after naturalizaiton, and γ-cellulose are remained supernatant part after naturalization.

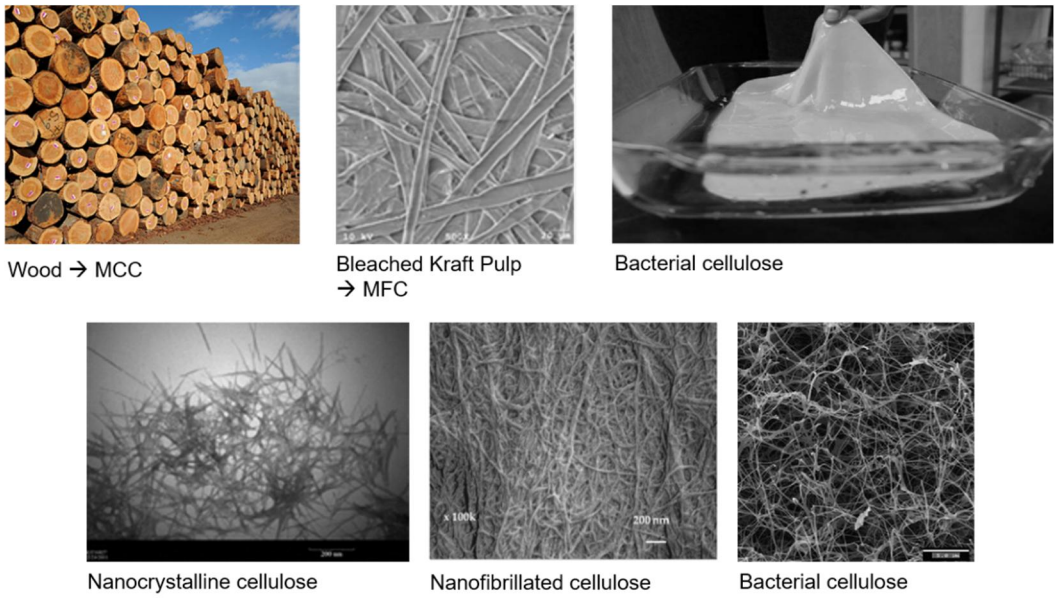

Figure 1.1.1. Several sources of a nanocellulose.

1.1.2. Examples of nanocellulose application

Due to the nano-sized diameter of nanofibrillated cellulose, the visible light can be passed without blocked.[9] It can be applied to GaAs electronics, bendable solar cell on nanocellulose substrate, cellulose nanocomposite based flexible organic light emitting diode (FOLED).[10] Nanocrystalline cellulose also absorb sound, and polarized optical properties, which can be applied diaphragm used in SONY headphones or polarized-light micrographs of NCC suspensions.[11] With silylation process, nanofibrillated cellulose us used to an oil absorption material.

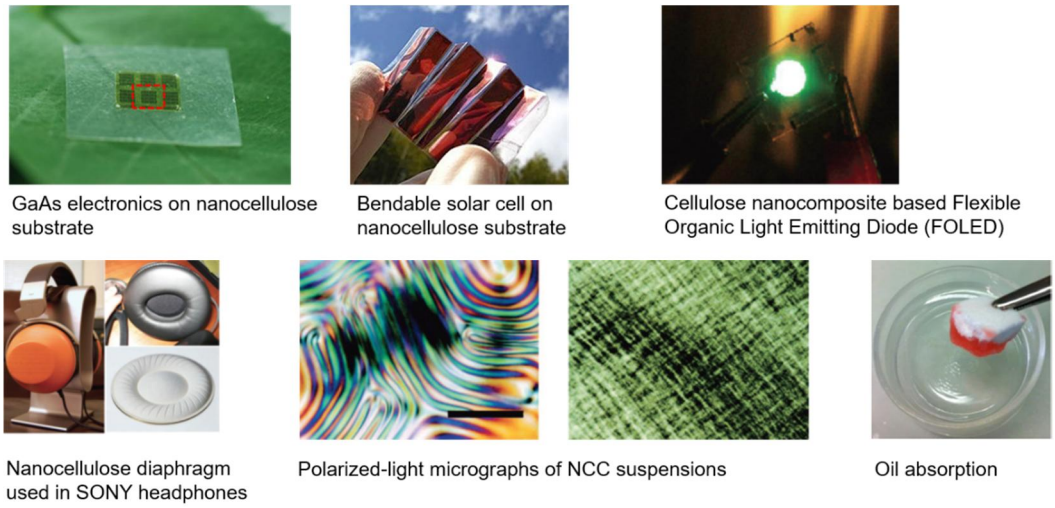

Figure 1.1.2. Examples of nanocellulose application.

1.2. What is flame retardancy?

1.2.1. Examples of fire catastrophe

In 1971, Daeyeongak Hotel fired due to combustible interior material, which is the worst hotel fired in the world. The first cause was a propane gas explosion, but the fire was easily move on the wood-based interior. In 2015, Uijeongbu apartment fired due to exterior material called Dryvit, which is made of expanded polystyrene foam, vulnerable to fire. In the case of other countries, USA nightclub fired due to PUF ignition in 2003. The cause of fire was the flame from a firework. In contrast, Dogok station arson in 2014, but it was failed due to flame retardant materials.

Daeyeongak Hotel fire in 1971 due to combustible interior material

Uijeongbu apartment fire in 2015 due to exterior material (Dryvit)

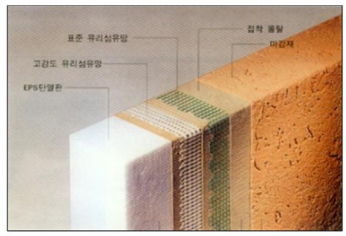

Dryvit is made of expanded polystyrene foam, vulnerable to fire.

2003 USA nightclub fire due to PUF ignition

Dogok station arson in 2014, failed due to flame retardant materials

Figure 1.2.1. Examples of fire catastrophe.

1.2.2. Burning mechanism

In the polymer matrix, burning mechanism has several zones depending on the state. The first step, the polymer has pyrolysis and thermal oxidation. After this step, it has gas decomposition step. The flame occurred with maximum heat, and then post combustion state proceeds (see **Figure 1.2.2**).

There are two phases on the boundary. One is condensed phase, produced charred residue via thermal degradation and thermal oxidation. The other is gas phase, which produced volatile products (see **Figure 1.2.3**).

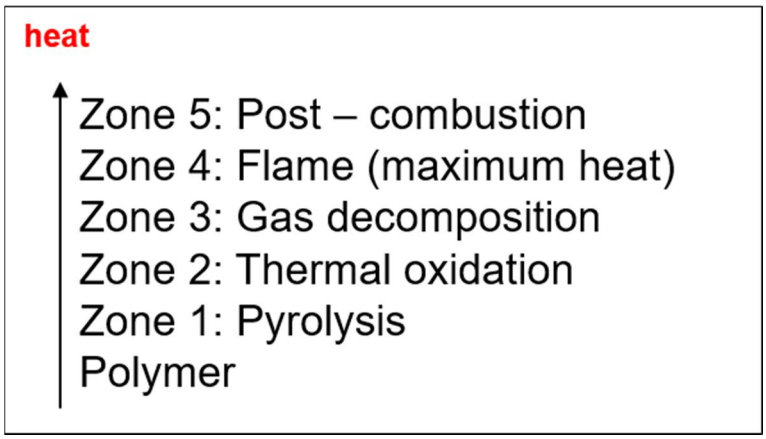

Figure 1.2.2. Burning mechanism of polymer matrix.

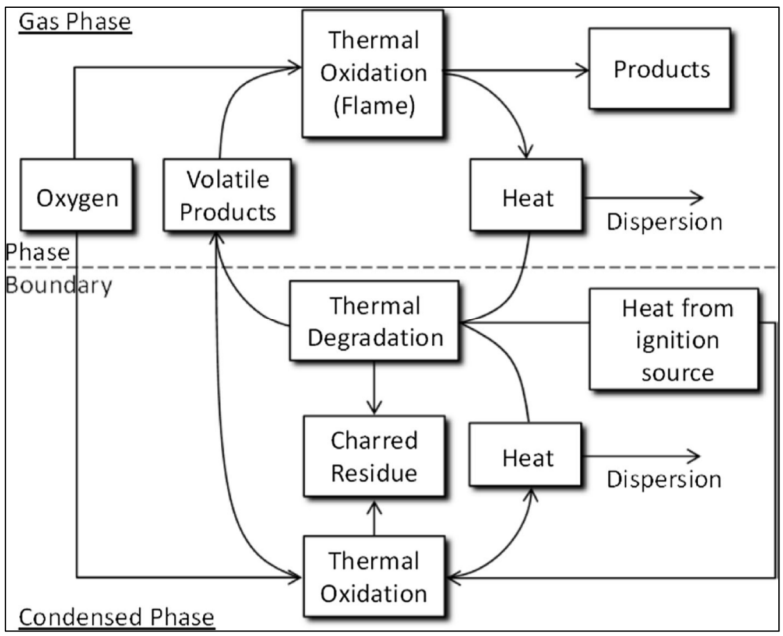

Figure 1.2.3. Burning mechanism of gas and boundary phase.

1.2.3. Limiting oxygen index (LOI)

The limiting oxygen index (LOI) is the minimum concentration of oxygen expressed as a percentage that supports combustion of the polymer. This is measured by passing a mixture of oxygen and nitrogen through a combustion specimen and decreasing the oxygen level until the critical level is reached. The value can be calculated by under equation.

$$\text{LOI} = \frac{vol.\ [O2]}{vol.\ [O2] + vol.\ [N2]} \times 100$$

Figure 1.2.4 shows LOI test machine. The importance of LOI is that it can be a criterion for determining self-extinguished in the air. The higher the LOI value, the more difficult it becomes to burn. **Figure 1.2.5** is the LOI value depending on the polymers. Since the oxygen concentration in the air is ~21%, if there is no flame in the high LOI value of the polymer matrix, the combustion is extinguished. Since the LOI value of polysilixane is 30, this polymer hardly burns. In this study, a nanocellulose were covered with polysiloxane layers to gain flame retardant properties using this principles.

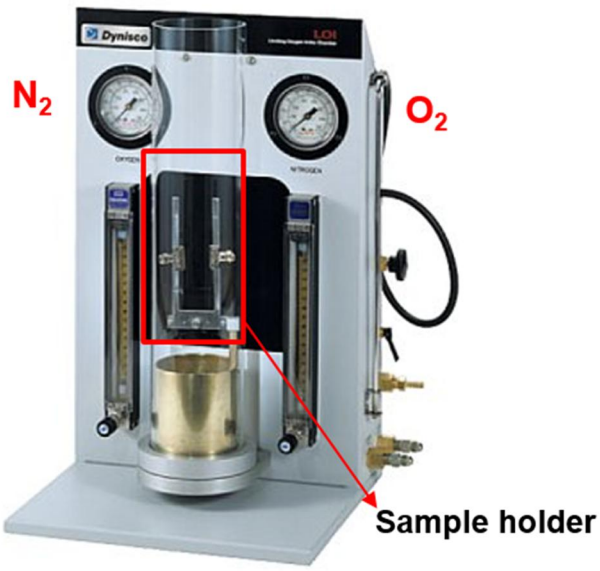

Figure 1.2.4. LOI test machine..

Polymer	LOI
Polyoxymethylene	15
Poly(ethylene oxide)	15
Poly(methyl methacrylate)	17
Polypropylene	17
Polyethylene	17
Polystyrene	18
Poly(1,3-butadiene)	18
Poly(vinyl alcohol)	22
Polycarbonate	27
Poly(phenylene oxide)	28
Polysiloxane	30
Poly(vinyl chloride)	45
Poly(vinylidene chloride)	60
Polytetrafluoroethylene	95

21%

Figure 1.2.5. LOI value depending on the polymers.

1.3. Objective of this study

In this study, a nanocellulose desinged for flame retardnacy with chemical treatment. Nanomaterials were fabricated with MTMS, which made polysiloxane layers on silylated nanocrystalline cellulose (Si-NCC) and silylated nanofibrillated cellulose. Si-NCC film cab be applied to flame retardant panel or wallpapers. Si-NFC can be used to poylmeric composite foam with conventional flame retardant materals to increase flame retardant properties such as limiting oxygen index, rate of heat release rate, and rate of somke release rate.

Chapter II.

Eco-friendly Nanocellulose Embedded Polymer Composite Foam for Flame Retardancy Improvement

2.1. Introduction

High flame retardancy is an essential property of commercial products used for the thermal insulation and building construction.[12,13] The products need to be designed to prevent heat transfer from outside and reduce the spread of fire from external heat sources, such as matches, kerosene heaters, electrical heaters, etc. Thus far, various engineering materials such as glass wools,[14] asbestos fibers,[15] silica aerogels,[16] and vacuum panels[17] have been used as fillers for thermal insulation in our daily lives and industrial applications. For practical applications, these materials, however, have disadvantages such as human toxicity, ecological persistence, and emission of carcinogens during unexpected combustion.[18] Furthermore, polymeric matrices, such as polystyrene and polyurethane possess a relatively high flammability.[19,20]

Cellulose is one of the most promising, attractive biopolymers in the world due to its lightweight,[21] low thermal conductivity,[22] eco-friendly feature,[23] low cost,[24] good biocompatibility,[25] and easy chemical treatment.[26,27] Nanocrystalline cellulose (NCC) is prepared by chemically or physically treating microcrystalline cellulose (MCC) obtained from various woods.[28,29] This material can be employed for preparation of construction materials,[30] thermal insulation,[31] hydrogel,[32] viscosity controlling agents,[33] tablets for pharmacy industry,[34] and bio-medical applications.[35] However, the flammability of NCC is a critical drawback for its

application to thermal insulation as a building material. On the other hand, chemical functionalization by using silylation[36] or phosphorylation[37] can allow NCCs to possess flame retardancy. Also, NCCs incorporated nanocomposites can achieve flame retardancy by combining with graphene oxide[38] or clay.[39] These can be employed as flame-blocking materials when they are filled between walls.

When NCCs are burned, carbonized char is produced and blocks propagation of flame. Silylation treatment of the NCCs can increase not only the amount of char produced but also improve flame retardant properties using silylated reaction.[39–41]

In this study, an eco-friendly flame retardant natural material was investigated. Flame retardant nanocrystalline cellulose (FR-NCC) was prepared by using a silylation method. Methyltrimethoxysilane (MTMS) and NCC were employed for preparation of the eco-friendly flame retardant. Effect of the silylation ratio was examined experimentally. Various characteristics of the FR-NCCs including morphology, thermal conductivity, chemical composition, and limiting oxygen index (LOI) were evaluated. The findings showed that the silylated NCCs had sufficiently high flame retardancy and low thermal conductivity compared with pristine NCCs.

2.2. Experimental

2.2.1. Preparation of Materials.

MCC and MTMS (97%) were purchased from Alfa Aesar. Sulfuric acid (95%) and hydrochloric acid (35%) were supplied by Daejung Chemicals, Republic of Korea. All chemicals were used as received without further purification.

NCC was prepared by using acid hydrolysis method.[3,42,43] 10.2 g of the MCC was dissolved in 100 mL of distilled water. The suspension was placed in an ice bath and stirred. Sulfuric acid was added dropwise up to a concentration of 63.5% (w/w) at 45℃ for 130 min. The suspension was rinsed with distilled water and centrifuged at least five times until pH 7 was reached, i.e., the supernatant was removed from the sediment and replaced with fresh distilled water, and then mixed again. The sample was sonicated for 30 min. and then lyophilized.

1 g of the lyophilized NCC was dissolved in distilled water. The suspension had a concentration of 0.5% (w/w) and then its pH was kept at 4 using HCl. The concentration of MTMS was varied based on the NCC weight, such as S1 (1 g NCC, 1 g MTMS), S2 (1 g NCC, 3 g MTMS), and S3 (1 g NCC, 5 g MTMS). The solution was transferred dropwise to the NCC solution and stirred for 2 h. The suspension was poured to a conical tube, and lyophilized. In each case, all other experimental conditions were held constant.

2.2.2. Characterization of Materials

Morphological structure of the samples was observed using a field-emission scanning electron microscope (FE-SEM, SU70, Hitachi, Japan). After the suspension was sonicated in a vial, it was dropped on a Si wafer and dried. After then, the sample was coated with Pt using a sputter (MSC-101, JEOL, Germany). SEM images were obtained using 3 kV secondary electrons.

Fourier transform infrared spectroscopy (FTIR) was employed to characterize the chemical structure of the samples. The FTIR spectra were recorded using a Varian 660 FTIR spectrometer eqipped with an Attenuated Total Reflectance Fourier Transform Infrared (ATR FTIR) mode. All data were acquired at a resolution of 4 cm^{-1} in the mid infrared region from 4000-650 cm^{-1} with 64 scans. The data were normalized from zero to one arbitrary unit to compare the intensities of the samples. The Varian Resolutions Pro software was employed to collect and analyze the data.

Thermogravimetric analysis (TGA) of the samples was carried out with a thermogravimetric analyzer (TA Instruments SDT Q600). Alumina crucible was used to hold the pressed powder sample of 20 mg. The sample was heated from room temperature to 600°C at a heating rate of 20°C/min under nitrogen flow of 100 mL/min. Each experiment was conducted at least twice to confirm the reproducibility.

The flame retardant properties of the samples were analyzed by measuring a limiting oxygen index (LOI) with a Stanton Redcroft flame meter according to the standard oxygen index test (ASTM D2863/77).

X-ray differential photoelectron spectroscopy (XPS) analysis was carried out using an AXIS-His electron spectrophotometer (Kratos Ltd., UK) with a monochromatic Mg Ka X-ray source (hυ = 1253.6 eV) with a power of 450 W. The powder samples were prepared on the Al substrate placed on the XPS sample holder. The samples were scanned under a high vacuum pressure of 5 x 10-10 torr at room temperature. A survey spectrum was recorded over a binding energy range of 0 to 1500 eV using a pass energy of 300 eV. The corresponding data analysis was performed by using the CasaXPS program for deconvolution of C1s and Si2p spectra, background subtraction, fitting, peak integration, and quantification of chemical elements. Since C was a dominant element in the spectra,

the charging effect induced by the C 1s peak of hydrocarbons was considered for the analysis. The curve fitting of spectrum peaks was conducted by combining the Gaussian distribution with the Lorentzian peak shapes.

The thermal conductivity of the samples was measured by using a thermal analyzer (C-Therm TCi, C-Therm Technologies Ltd, New Brunswick, Canada). The inner size of mold was 23 mm in diameter and 6 mm in height.

2.3. Results and discussion

2.3.1. Morphology and chemical structure of silylated NCC

Pristine NCC and silylated NCC with different contents of MTMS were prepared. SEM images were taken to grasp the amount of polysiloxane layer covered on NCC among the fabricated samples. **Figure 2.3.1 (a)** shows a needle-like structure of NCCs obtained via acid hydrolysis. As shown in **Figs. 2.3.1 (b) to (d),** the diameter of the NCCs increased as the amount of silylation increased. This is due to the formation of a polysiloxane layer on the NCC surface. The layer can increase the hydrophobicity of the NCC surface by removing the hydroxyl group. The silylation level of the samples was measured by using XPS (**Table 2.3.1**). The amount of silylation was evaluated with Si weight percent (Si wt%). The Si wt% increased with increase in the degree of silylation. The Si wt% varied from 0 to 25 wt%.

The surface silylation of NCCs was confirmed by the FT-IR analysis as shown in **Figure. 2.3.2**. The broad band around at 3400 cm^{-1} originates from the hydroxyl group of the NCC. The intensity of the -OH peak decreased with the addition of the MTMS due to the silylation. This supports that the Si-O-C linkage was formed on the backbone of the NCC. The peaks at 2975 and 2896 cm^{-1} are allocated to the asymmetric C-H stretching mode of the Si-CH_3 and C-H stretching mode, respectively. The area percentage of these peaks diminished from **Figure. 2.3.2 (a) to (d)**. As the silylation progresses, the area percentage of -CH_3 picks tends to decrease since the amount of Si-O-Si is relatively higher than that of -CH_3 picks.[44] The peak intensities at 1271 cm^{-1} and 778 cm^{-1} are imparted to the Si-C and Si-O-Si bonding, respectively. These intensities increased with increase in the amount of MTMS. The absorption band for the Si-O-Si bonds is overlapped in the 1000 – 1100 cm^{-1} region with the C-O bonds of the NCC. **Figure 2.3.2** shows that the intensities of the C-H peak and Si-O-Si peak increased with increase in the weight percent of MTMS, resulting in higher hydrophobicity than pristine NCC. Additionally, the resulting Si-C group can increase flame retardant properties.

XPS scans of C1s and Si2p were performed to confirm chemical composition of the samples. **Figure 2.3.3 (a)** shows that the deconvolution of the C1s provides four

peaks for the NCC sample. The first peak at 284.5 eV indicates a carbon linkage and/or hydrogen atoms. The second peak at 286.1 eV corresponds to the carbon atom bonded to hydroxyl group, which has the largest area fraction of the others due to its abundant -OH groups on the cellulose structure. The third peak at 287.6 eV relates to a carbon atom bound to an oxygen atom. The firth peak at 288.7 eV represents a carbon atom bound to two noncarbonyl oxygen atoms.[45] As shown in **Figure. 2.3.3 (b) to (d),** a new peak ranging from 282.5 through 286.6 eV indicated a carbon atom bonded to a single silicon atom. This siliceous carbon is produced due to the formation of Si-C bond between the NCC and MTMS solution. In addition, the area ratio of each Si-C peak increased from 35.5% to 56.1%. It is evident that the silylation was successfully carried out, which are in coincidence with the FTIR data.

The XPS scan results of Si2p indicated that the S1, S2, and S3 samples had two main peaks (**Figure. 2.3.4 (a) to (c)**). The first peak ranging from 100.2 to 100.3 eV for all the samples represents a silicon/carbon bonding. The second peak at 101 eV is attributed to a silicon/oxygen bonding. The highest intensity of S3 at 101 eV is due to the silylated moiety of NCC surface. Increment in the area percent of Si-O means that more polysiloxane layers are produced on the NCC surface. As a result, it can be seen that the layers increase with increase in the amount of silylation.

Table 2.3.1. XPS chemical composition of NCC and silylated NCC.

Sample name	Peak	Atomic percent (%)	Mass percent (%)
NCC	C 1s	56.46	49.33
	O 1s	43.54	50.67
S1	Si 2p	8.14	14.99
	C 1s	43.48	34.24
	O 1s	48.38	50.76
S2	Si 2p	10.01	18.09
	C 1s	41.86	32.35
	O 1s	48.13	49.56
S3	Si 2p	14.64	25.09
	C 1s	34.59	25.35
	O 1s	50.77	49.56

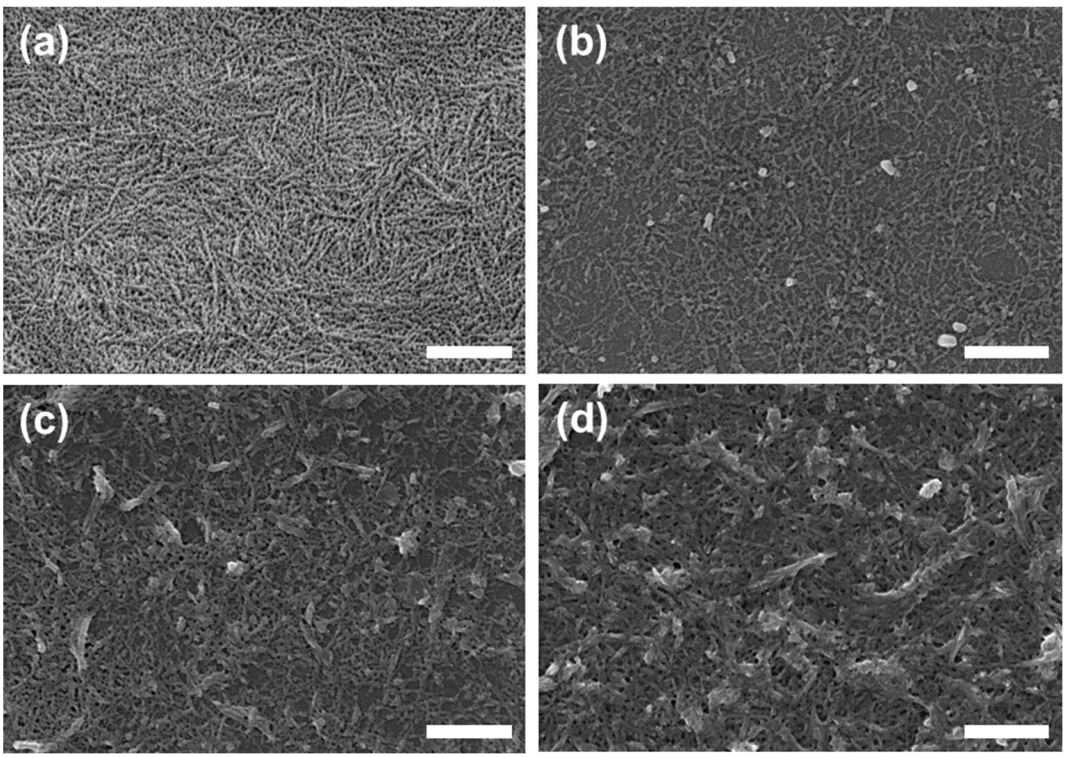

Figure 2.3.1. SEM images of (a) pristine NCC, (b) S1, (c) S2, and (d) S3 samples (Scale bars: 500 nm).

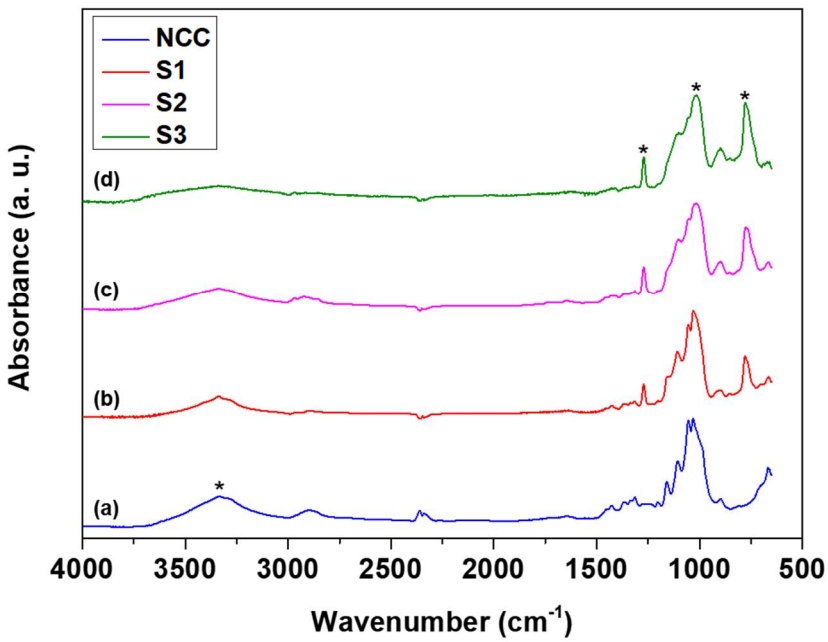

Figure 2.3.2. FTIR spectra of NCC samples in various conditions.

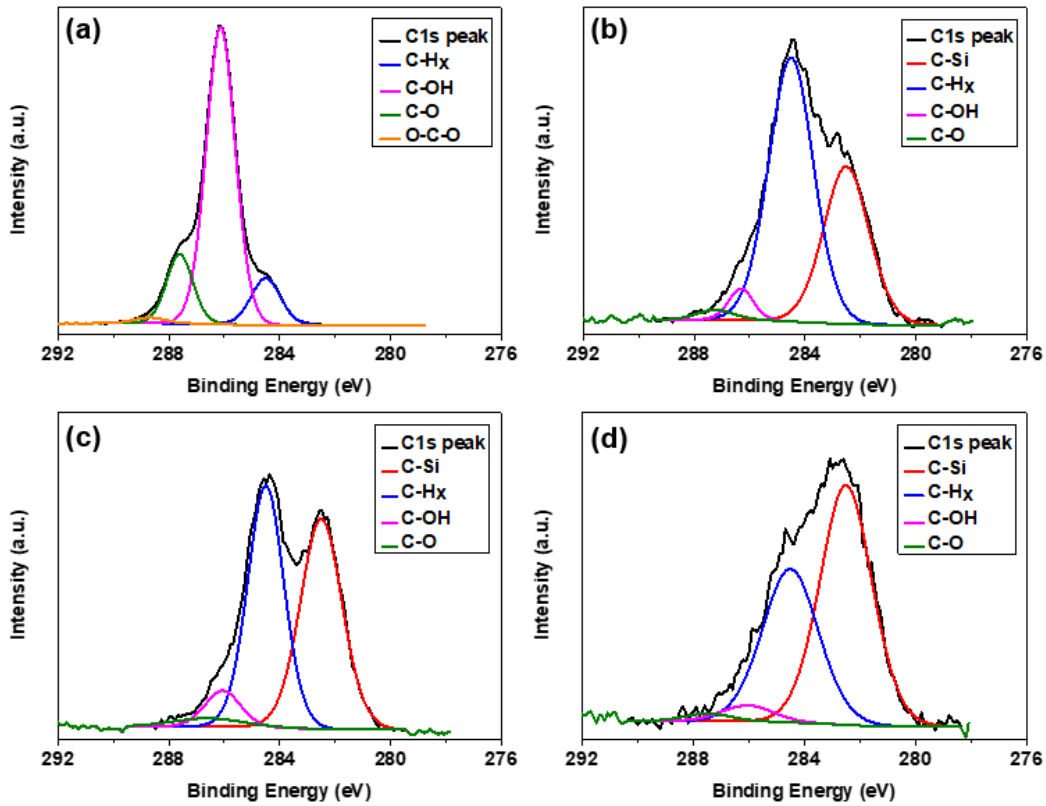

Figure 2.3.3. XPS Curve fitting of C1s spectra for (a) NCC, (b) S1, (c) S2, and (d) S3.

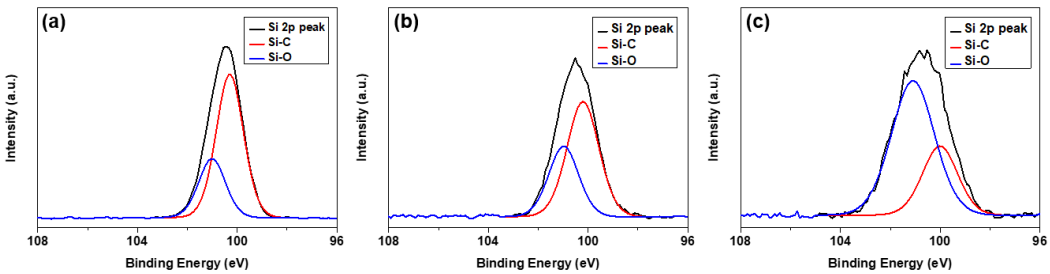

Figure 2.3.4. XPS Curve fitting of Si2p spectra for (a) S1, (b) S2, and (c) S3.

2.3.2. Chemical structure of char

Chemical structures of the char formed from the samples were identified by FTIR analysis as presented in **Figure. 2.3.5**. In the case of the S3 char, the peak at 2970 cm^{-1} was formed by the bond between NCC and MTMS, i.e., the C-H vibration mode of the Si-CH_3. On the other hand, the NCC char did not show a peak around 2970 cm^{-1}. Due to the polysiloxane bonding of S3, two peaks at 1135 and 1035 cm^{-1} were identified in the S3 char. The S3 char also exhibited the Si-C bond at 775 cm^{-1}. The peak of MTMS at 1200 cm^{-1} represented the Si-O bond.

Chemical composition of the char was also investigated by using XPS. A pyrolysis of the cellulose is proceeded by the complex pathways.[46–49] Firstly, the cellulose is decomposed to volatile tars due to an intermolecular dehydration. Low molecular weight volatiles are also formed due to depolymerization and the levoglucosan is emitted as a result. Finally, a carbonaceous residue is generated after decomposition. The NCC used in this experiment produces more levoglucosan since hemicelluloses are removed by acid-treatment with use of H_2SO_4. **Figure 2.3.6 (a)** represents the results of the S1 char. Compared with the peaks of the S1 char, the peaks of the S3 char possess similar intensities of carbide and hydrocarbon peaks (see **Figure. 2.3.6 (b)**). However, the proportion of carbons bound to the oxygen peak increased slightly. **Figure 2.3.6 (d)** shows that the peak of carbide is higher than that of the peak in **Figure. 2.3.6 (c)**. The detailed information is tabulated in **Table 2.3.2** for the S1 and S3 char, respectively. The first peak at 100.2 eV indicates that the peak of Si-C bonding is the same as the peak of silylated NCC. The second peak ranging from 101.4 eV to 101.5 eV represents dialkoxysilane ($Si(O)_2$).[45,50] This trend alludes that the primary silane moiety can be hydrolyzed and Si(-C2)($-O_2$) is produced during the NCC pyrolysis. The last peak in the vicinity of 103.2 eV corresponds to the silicon oxide (Si($-O_4$)) peak. Since more silylation was applied to the S3 sample, larger amounts of silicon-related compounds were produced in the S3 char. The XPS results indicate that silylation of NCC accelerates char formation by lowering the decomposition rate of NCC and generating silicon oxide.

Table 2.3.2. XPS Si2p spectra of S1 char and S3 char.

(a) S1 char

Binding energy (eV)	Area (%)	Structure
100.3	9.1	Si-C
101.5	70.2	$Si(-O)_2$
103.0	20.7	$Si(-O)_4$

(b) S3 char

Binding energy (eV)	Area (%)	Structure
100.2	65.9	Si-C
101.4	19.3	$Si(-O)_2$
103.2	14.8	$Si(-O)_4$

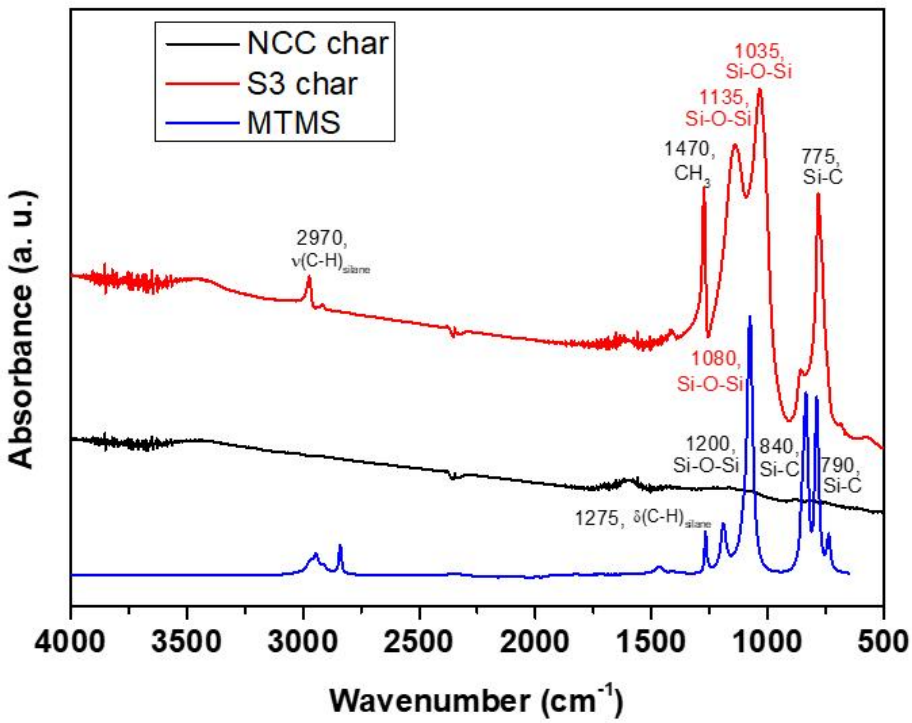

Figure 2.3.5. FT-IR spectra of chars: (a) NCC char (b) S3 char, and (c) MTMS.

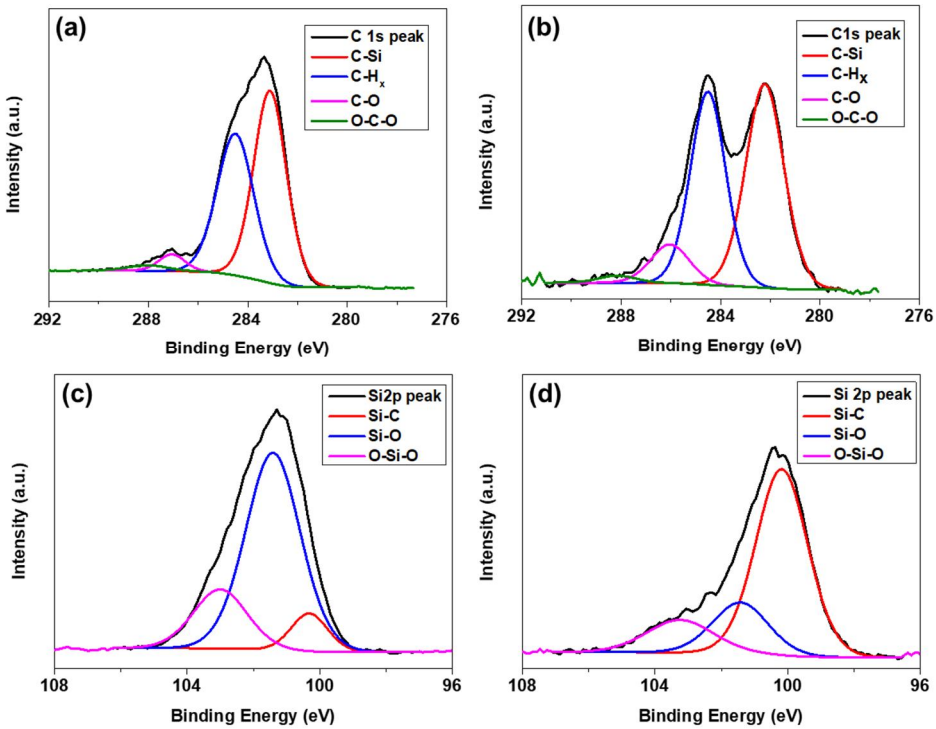

Figure 2.3.6. XPS Curve fitting of C1s spectra for (a) S1 char, (b) S3 char, Si2p spectra of (c) S1 char, and (d) S3 char.

2.3.3. Flame Retardancy of silylated NCC

The thermal stability of the pristine NCC and silylated NCCs was examined by using TGA (see **Figure. 2.3.7**). As shown in **Figure. 2.3.7 (a)**, thermal stabilities of the samples were improved by silylation. At the ignition stage up to 100℃, the residual weight slightly decreased due to moisture that the NCC owns naturally. The NCC was decomposed rapidly in the temperature range from 150℃ to 210℃, but the samples containing silylated NCC degraded more slowly than the pristine NCC since high bonding energy of Si-C delays thermal decomposition. At the last stage in the temperature range from 210℃ to 600℃, the decomposition rate of the pristine NCC became faster than that of the silylated NCCs by forming the char. The silylated NCC could promote the formation of silicon carbide and SiO_2, and thus thermal stability increased.

Flame retardant materials can prevent pyrolysis by acting as a thermal insulator and mass transport barrier to the volatile products generated during decomposition. The S3 sample has the lowest decomposition rate than the other samples due to the highest silylation ratio in the siliceous carbon. More silylation than that of the sample S3 has no effect on the thermal stability of the samples, which is identified in **Figure. 2.3.8**. **Figure 2.3.8 (b)** indicates that the inflection point of samples increased from 192℃ to 226℃ after silylation. As the silylated weight percentage increased, the inflection points increased. As shown in **Figure. 2.3.7 (c)**, the weight fraction of char residue increased from 29% to 80% and the thermal stability was improved at high temperature. The char blocked the flame and protected internal material from burning. This phenomenon occurred since the silylated NCC delayed thermal decomposition.

LOI testing was conducted to investigate the flammability of the samples in air environment. The LOI parameters are generally used to evaluate the flammability of fiber or plastic products. It was shown from **Figure. 2.3.9** that the NCC had an LOI value of 18.4%. This implies that it could be ignited easily and quickly in an open atmosphere. However, the samples with LOI values higher than 21% were burned slowly even in the air. Depending on the silylation ratio, the LOI values increased to 20.2% (S1), 27.2% (S2), and 34.2% (S3). The LOI value of the S3 was about 60% higher than weight fraction of oxygen in the air (21%).

Figure 2.3.10 shows a photograph of the sample prepared after dispersing the S3 in water and drying. Before burning, the S3 shown in **Figure. 2.3.10** was ignited for 30 s. The area covered by the flame did not spread out. There was no significant change in the morphology of samples even if the ignition time was increased. Only the surface of the S3 was scorched in **Figure. 2.3.10** after burning, and the other part was not damaged by flame (see the red circle). This is because the S3 blocks the propagation of fire and prevents the flame from expansion.

Thermal conductivity of the sample is shown in **Figure. 2.3.11**. The thermal conductivity increased as the amount of silylation decreased. The pristine NCC had a thermal conductivity of 49.2 $W \cdot m^{-1} \cdot K^{-1}$, which is relatively higher than those of other celluloses due to the NCC crystalline structure. The S3 had a thermal conductivity of 45.9 $W \cdot m^{-1} \cdot K^{-1}$, which is 7% lower than that of the pristine NCC due to the polysiloxane structure on the surface of the S3. On the other hand, the thermal conductivity of MTMS aerogel thin film is 19 $W \cdot m^{-1} \cdot K^{-1}$.[22] The MTMS aerogel can reduce the thermal conductivity of the silylated NCC. The thermal conductivity of the S3 sample was higher than that of air (26 $W \cdot m^{-1} \cdot K^{-1}$), but lower than that of pristine NCC. Therefore, it can be used as an interior material when constructing a passive house to reduce heat transfer.

The apparent density of the powder samples was around 60 kg/m^3 in this experiment. In general, decreasing the diameter at the same density lowers the effective thermal conductivity. The silylated NCC shows a lower thermal conductivity than that of cellulose. Hence, it can effectively block heat transfer when used as a filler between walls. On the other hand, if condensation of water occurs in the thermal insulation material, its thermal insulation property decreases. Since the coefficient of thermal conductivity of water is much higher than that of air, the moisture in the insulation material has a fatal effect on the thermal performance. We expect that this problem could be solved by using a hydrophobic nanocellulose with high flame retardancy and thermal insulation feature.

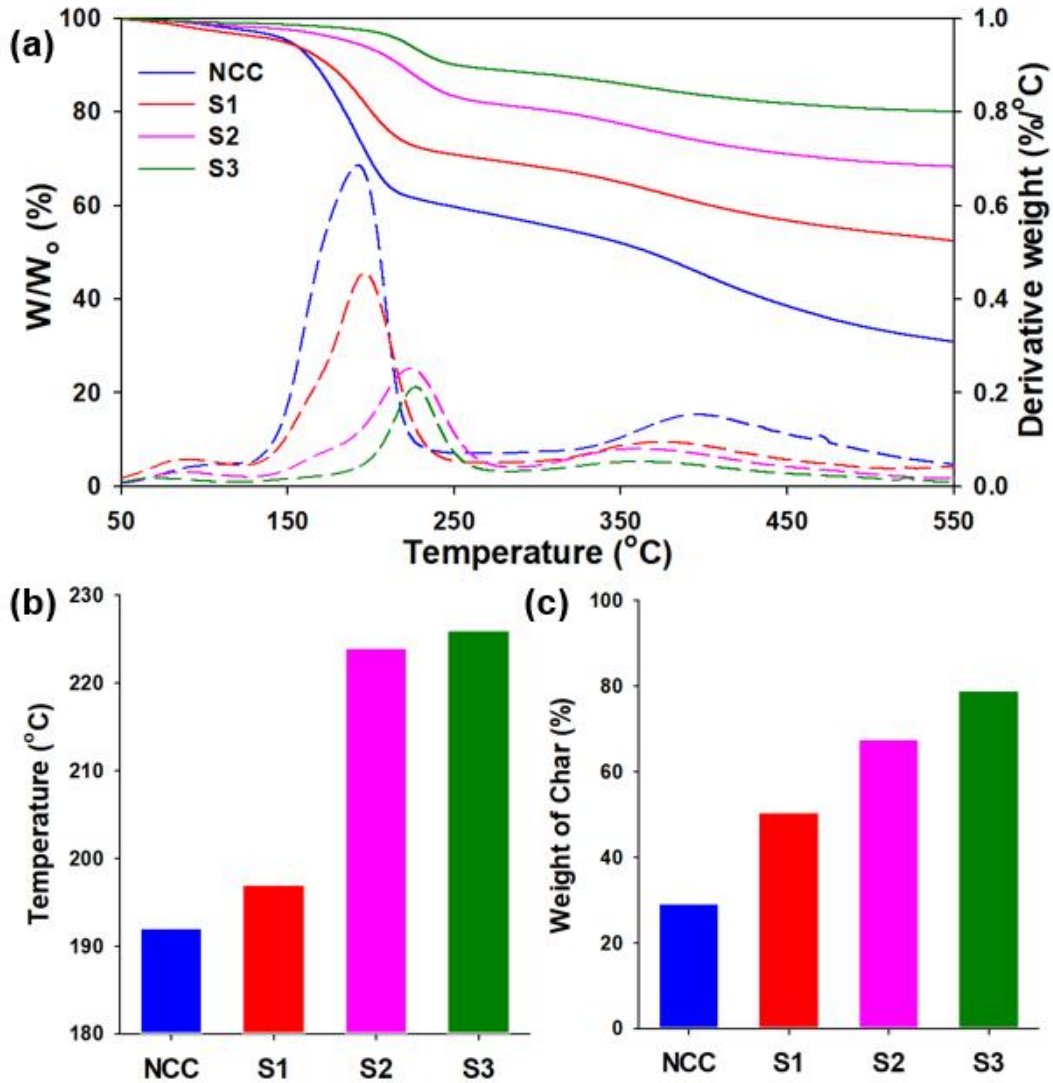

Figure 2.3.7. Thermal stability of the samples prepared in this study: (a) TGA and dTGA thermograms of pristine NCC, S1, S2, and S3 in N_2 atmosphere at 600℃, (b) inflection points of dTGA curve, and (c) weight of char residue for the samples.

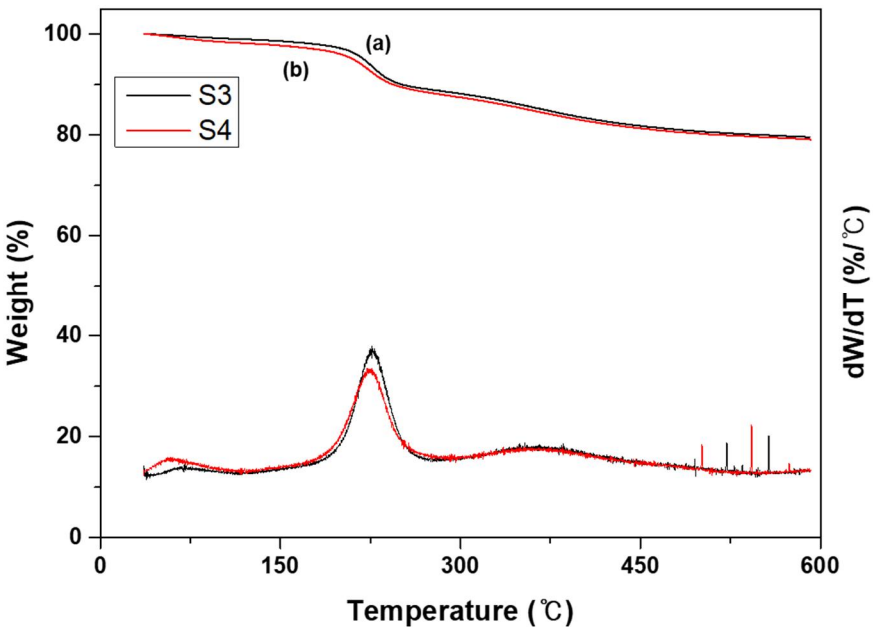

Figure 2.3.8. TGA and dTGA thermograms of samples: (a) S3 (1 g of NCC, 5 g of MTMS) and (b) S4 (1 g of NCC, 7 g of MTMS).

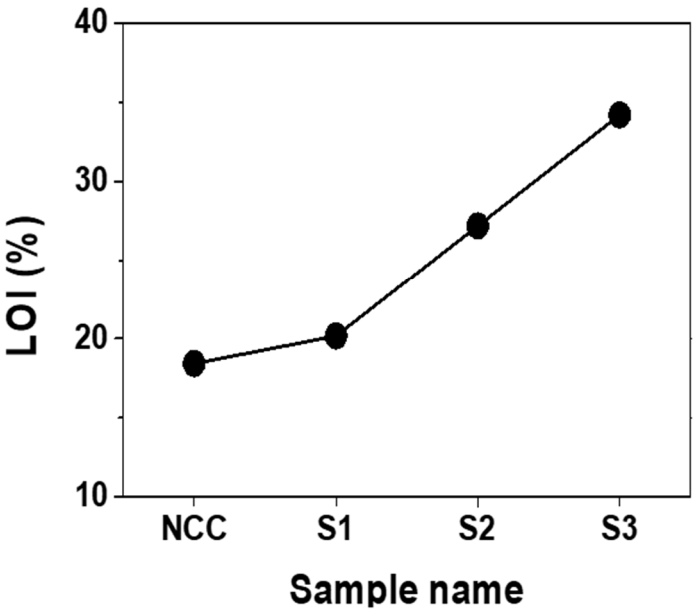

Figure 2.3.9. Analysis of flame retardancy: LOI test of pristine NCC, S1, S2 and S3.

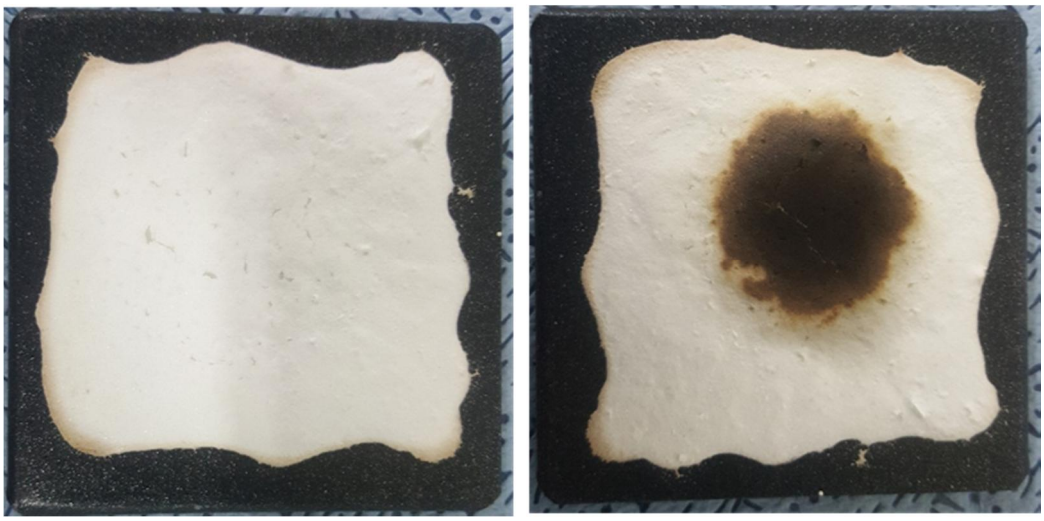

Figure 2.3.10. Analysis of flame retardancy: photographs of S3 sample after burning test (left: before burning, and right: after burning). The size of the black plate is 8 cm.

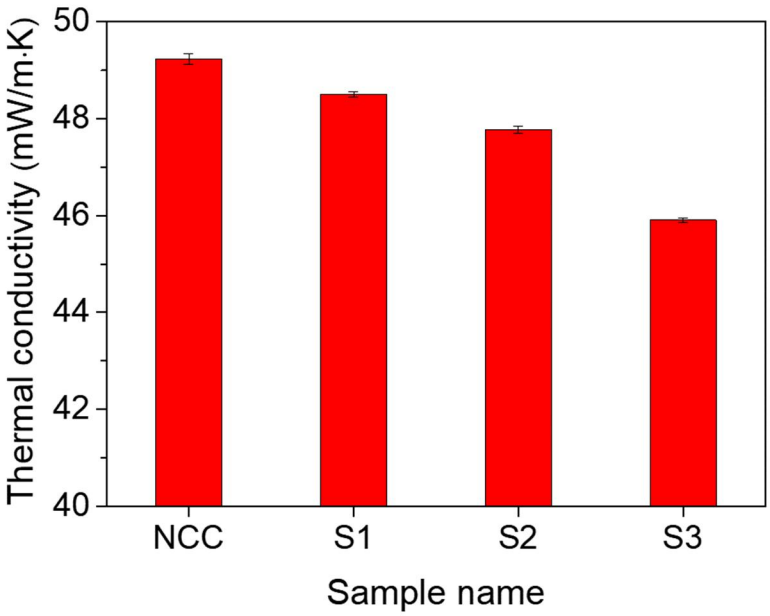

Figure 2.3.11. Thermal conductivity of NCC and silylated NCCs.

2.4. Conclusions

We fabricated flame retardant, and lightweight nanocellulose via facile, effective chemical treatment. The silylation process was optimized by controlling the amount of MTMS treatment on the NCC surface. The results showed that the optimal mass ratio of NCC and MTMS was 1:5 for the S3 sample. The thermal degradation was investigated through TGA. The data revealed that the S3 sample had higher thermal stability than the others, which implies that silylation delays the rate of thermal degradation of the NCC. The thermal conductivity of the treated samples decreased. It was found that the amount of residual char increased with increasing the content of MTMS. The chemical composition of the char was investigated by using FTIR and XPS. The finding showed that silicon oxide and silicon carbide formed during the pyrolysis process promoted the formation of the siliceous char layer resulting in high LOI value. It is expected that the FR-NCC developed in this study provides a new insight into flame retardant material and a possibility of an ecofriendly biomaterial-based flame retardant.

Chapter III.

Flame retardant composite foam modified by silylated nanocellulose and tris(2-chloropropyl) phosphate

3.1. Introduction

Polymeric foams are widely used in many applications, such as building interior materials,[13] insulation materials, refrigeration,[51] and sound absorbers[52] due to their low thermal conductivity and low density. These materials are facing daunting problems of high flammability and generation of smoke during combustion.[53] Both flame and smoke definitely threaten people's lives in fire disaster.[54] In order to overcome these problems, flame retardant fillers have been incorporated in polymeric foams, such as clay,[39] silicon containing structure,[55] halogen compounds,[56] intumescent materials,[57] composites,[58] graphene oxide,[59] and chemically treated nanocellulose.[60] Among these materials, halogen based flame retardants are the most traditional option because they are readily mixed with polymeric matrix and economically affordable.

Tris(2-chloropropyl) phosphate (TCPP) does not significantly change the viscosity of polyurethane resin when the liquid material is added.[61] This is a helpful characteristic for fabricating a uniform-cell-sized polyurethane foam (PUF) compared with other solid flame retardant materials. However, it generates radicals during combustion, which impede burning of the polymer matrix and release incompletely-burnt black smoke.[62]

Nanocellulose is a widely used filler for polymeric composites owing to its

lightweight,[63] low thermal conductivity,[64] easy chemical treatment,[26] good biocompatibility,[25] and eco-friendly feature.[65] While cellulose is generally flammable, it must be used as a flame retardant only after chemical treatment. In the previous study, we reported that silylation on the nanocellulose surface yields flame retardacy.[66] Silylated nanocellulose produces siliceous char layer during combustion, which prevents heat transfer from the outside and protects the inner polymeric matrix.

Combining silylated and nanofibrillated cellulose (Si-NFC) with PUF/TCPP can help solve the smoke problem of halogen-based flame retardants during combustion. The underlying mechanism is quite similar to the mechanism of clay and modified silicate. However, the density and color of the composite are not remarkably changed due to the lightweight and white color of nanocellulose, respectively.[67]

In this study, we produced flame retardant PUF composites using TCPP and Si-NFC. NFC was treated with methyltrimethoxysilane (MTMS) for silylation. The pristine PUF, PUF with TCPP, PUF with Si-NFC, and PUF/TCPP/Si-NFC composites were prepared and assessed. The ratio of TCPP and Si-NFC to PUF was controlled to maintain the processability of the PUF foam. The morphology of microstructure, chemical structure, thermal properties, and flame retardant properties were investigated through field-emission scanning electron microscopy (FE-SEM), Fourier transform infrared spectroscopy (FTIR), thermogravimetric analysis (TGA), limiting oxygen index (LOI), and cone calorimeter tests. The residual char was also analyzed to evalute the flame retardancy and thermal decomposition.

3.2. Experimental

3.2.1. Materials

Nanofibrillated cellulose (NFC) was purchased from the University of Maine, USA. Methyltrimethoxysilane (MTMS, 97%) were obtained from Alfa Aesar, Republic of Korea. Tris(2-chloroisopropyl) phosphate (TCPP) were supplied by Cellchem International, USA. Polyether polyol (MCNS Rigid system polyol) and Methylene diphenyl diisocyanate (MDI, M200) were provided by MCNS, Republic of Korea. All chemicals were used as received without further purification.

3.2.2. Preparation of Materials

1 g of the lyophilized NFC was dissolved in distilled water. The suspension had a concentration of 0.5% (w/w) and then its pH was kept at 4 by using HCl. The mixing weight of MTMS was varied based on the NFC weight: N1 (1 g NFC, 1 g MTMS), N2 (1 g NFC, 3 g MTMS), and N3 (1 g NFC, 5 g MTMS). The MTMS was transferred dropwise to the NFC solution and stirred for 2 h. The suspension was poured into a conical tube and lyophilized for 3 days. In each case, all other experimental conditions were held constant.

Reactant A containing polyol, water, foaming agent, catalyst, surfactants, etc. and Reactant B including isocyanate were mixed by a high speed blade at 3000 rpm for 10 seconds. TCPP and Si- NFC were also mixed by following the ratio listed in **Table 3.3.1**. PUF1 was a pristine sample, and PUF2 was mixed with 20% TCPP. 5% Si-NFC was added to PUF3, and 20% TCPP and 5% Si-NFC were added to PUF4. The density of the PUFs was fixed at 50 kg/m^3. The mixture was infused into a mould to manufacture a desired-shape sample (mold size : 100 × 100 × 50 mm^3). The produced foams were kept at room temperature for the post curing for more than 7 days.

Table 3.2.1. Content of TCPP and Si-NFC in the PUF samples.

Sample name	TCPP (wt%)	Si-NFC (wt%)
PUF1		
PUF2	20	
PUF3		5
PUF4	20	5

3.2.3. Characterization of Materials

The morphological structure of the sample was observed using a field-emission scanning electron microscope (FE-SEM, SU70, Hitachi, Japan). After then, the sample was coated with platinum by using a sputter (MSC-101, JEOL, Germany). SEM images were obtained using 3 kV secondary electrons.

Fourier transform infrared spectroscopy (FTIR) was employed to characterize the chemical structure of the samples. The FTIR spectra were recorded using a Varian 660 FTIR spectrometer (Agilent, USA) equipped with an Attenuated Total Reflectance Fourier Transform Infrared (ATR FTIR) mode. All the data were acquired at a resolution of 4 cm^{-1} in the mid infrared region from 4000 - 650 cm^{-1} with 64 scans. The data were normalized from zero to one arbitrary unit to compare the intensities of the samples. The Varian Resolutions Pro software (Agilent, USA) was employed to collect and analyze the data.

The thermogravimetric analysis (TGA) of the samples was carried out with a thermogravimetric analyzer (TA Instruments, Discovery TGA, USA). An alumina crucible was used to hold the pressed sample of about 20 mg. The sample was heated from room temperature to 700°C with a heating rate of 20°C/min under nitrogen flow of 100 mL/min. Each experiment was conducted at least twice to confirm the reproducibility.

The flame retardant properties of the samples were analyzed by measuring a limiting oxygen index (LOI) with the Stanton Redcroft flame meter (UK) according to the standard oxygen index test (ASTM D2863/77).

The cone calorimeter test was conducted for composite polyurethane foams according to the test standard (ISO 5660 standards, ASTM E 1354) with a cone calorimeter (Festec International Co. Ltd., Korea). All samples were conditioned at room temperature and relative humidity of 45% for more than 2 weeks prior to testing. The samples were exposed in the horizontal orientation to an irradiance of 50 kW m−2 upon opening the thermal shutter and imposing an electric spark for piloted ignition. The sample size for the measurement was set at 100 × 100 × 50 mm^3.

The thermal conductivity of the samples was measured by using a thermal

analyzer (C-Therm TCi, C-Therm Technologies Ltd, New Brunswick, Canada). The dimension of the cylindrical mold was 23 mm in diameter and 6 mm in height.

3.3. Results & Discussion

3.3.1. Morphology and chemical structure

The density and cell size of the foams are the major factors to affect the performance of the foams, such as mechanical property,[68] structural stability,[69] thermal conductivity,[70] and electromagnetic shielding.[71] The composite polyurethane foams (PUFs) with tris(2-chloropropyl) phosphate (TCPP) and silylated and nanofibrillated cellulose (Si-NFC) were fabricated as listed in **Table 3.3.1**. The SEM images of the PUFs were obtained to confirm the fabricated products and the morphology of the cell structures (**Figure 3.3.1**). As shown in **Figure 3.3.1(a-d)**, all the samples have almost the same volume. In general, when a large amount of flame retardant materials are added to the foam, the foaming process can be interrupted and the dimensional stability of the foam decreases.[72] That is, these retardant materials deteriorate the cell formation, and induce the post shrinkage and the collapse of foam strut.

Density of the foam was fixed at 50 kg/m^3 for entire experiments. **Figure 3.3.2** shows the cell morphology of the samples. The average cell diameter tended to increase along with the addition of TCPP. The cell diameter of the samples containing TCPP increased by 10% compared with that of the other samples because the liquid flame retardant material had detrimental effect on the cell structure formation. However, PUF3 and PUF4 had lower average diameters than PUF1 and PUF2. Since Si-NFCs acted as a nucleation agent, formation of the cellular structure was facilitated.[73] As a result, the cell formation rate was determined by the competition between those two factors.

Figure 3.3.3 shows the morphology of NFCs and Si-NFCs. The pristine NFCs had fine web-like structures and high aspect ratio, which is suitable for acting as a nucleation site. The diameter of the NFCs increased as the amount of silylation increased. N3 was finally selected in the experiments because of the presence of accumulated polysiloxane layers on the surface of the NFCs. These Si-NFCs acted as a foaming agent as well as a flame retardant material.

FTIR analysis was conducted to verify formation of the urethane linkages and chemical structure of the composite samples as shown in **Figure 3.3.4**. The broad band

around 3400 cm^{-1} was due to the hydroxyl group originated from the polyol (**Figure 3.3.4a**). A peak at 1711 cm^{-1} was allocated to C=O of the urethane and ester groups of the polyol. The bands at 1510 and 1410 cm^{-1} regions indicated the characteristics of a urea linkage. The resulting characteristic peaks of the PUFs were observed at 2970, 2873, 1595, and 1067 cm^{-1} indicating CH_3 vibration, CH_2 vibration, aromatic ring, and C-O bond, respectively.[74] Considering the molecular structure of TCPP in the PUF2 and PUF4, the phosphorus related peaks at 1075, 1016, and 750^{-1} cm confirmed P=O, P=O, and P-C bonds, respectively (**Figure 3.3.4b**). The absorption band for the Si–O–Si bond was overlapped in the 1000–1100 cm^{-1} region due to the moiety of Si-NFCs in the cases of PUF3 and PUF4 (**Figure 3.3.4c** and **4d**).[75] This finding showed that the liquid flame retardant material, TCPP, still existed inside the PUF cell structure.

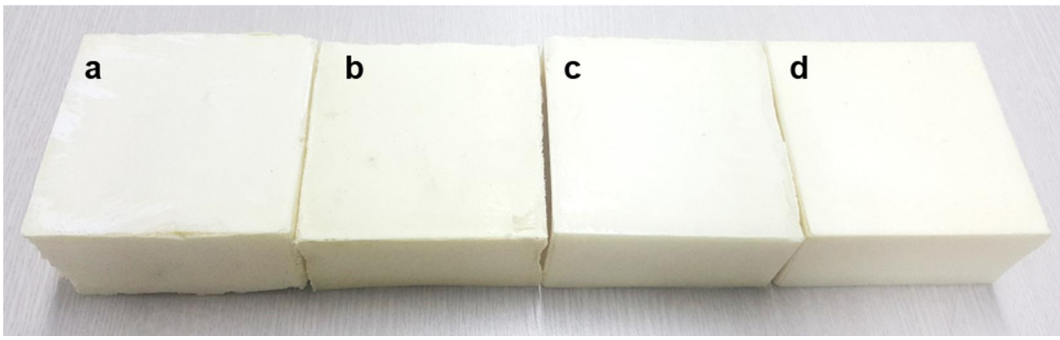

Figure 3.3.1. Photographs of (a) PUF1, (b) PUF2, (c) PUF3, and (d) PUF4 (sample sizes : 10 cm x 10 cm x 5 cm).

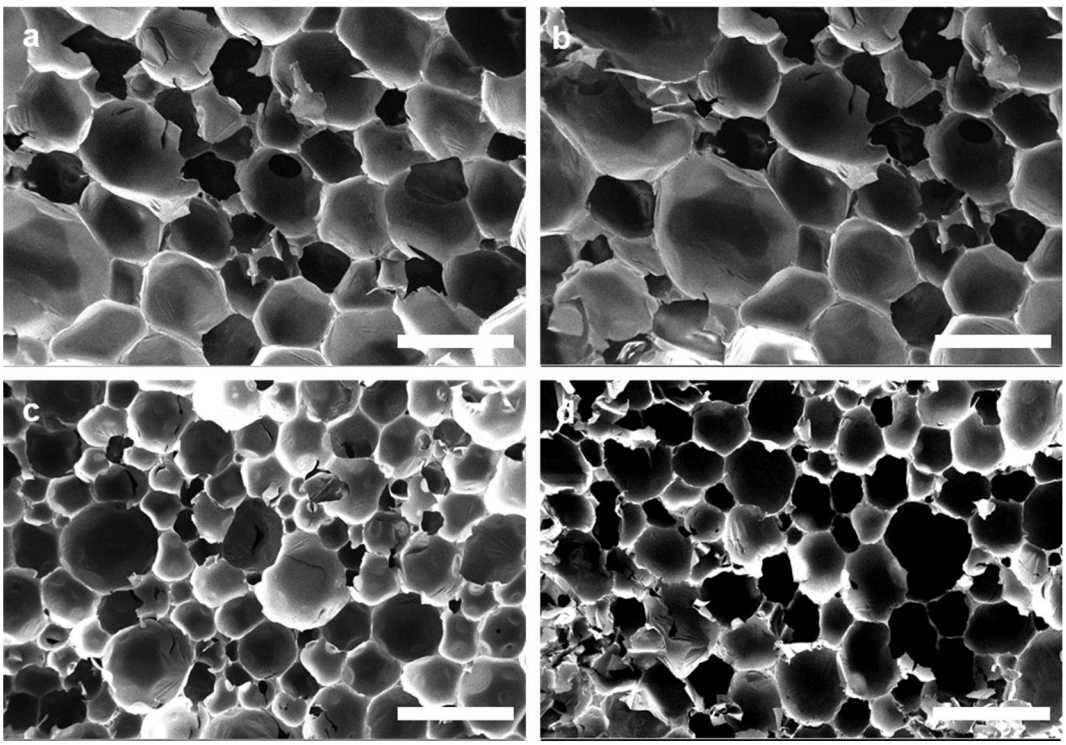

Figure 3.3.2. SEM images of (a) PUF1, (b) PUF2, (c) PUF3, and (d) PUF4 (scale bars : 500 μm).

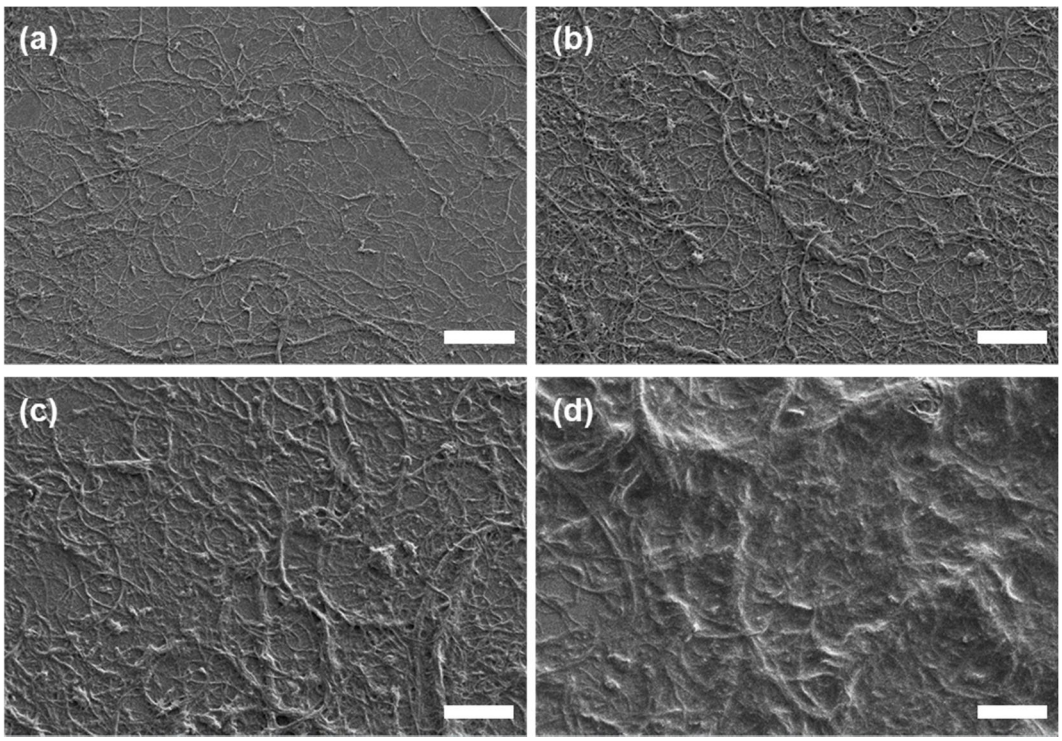

Figure 3.3.3. Morphology of samples in this study: (a) pristine NFC, (b) N1, (c) N2 and (d) N3 (scale bars : 2 μm).

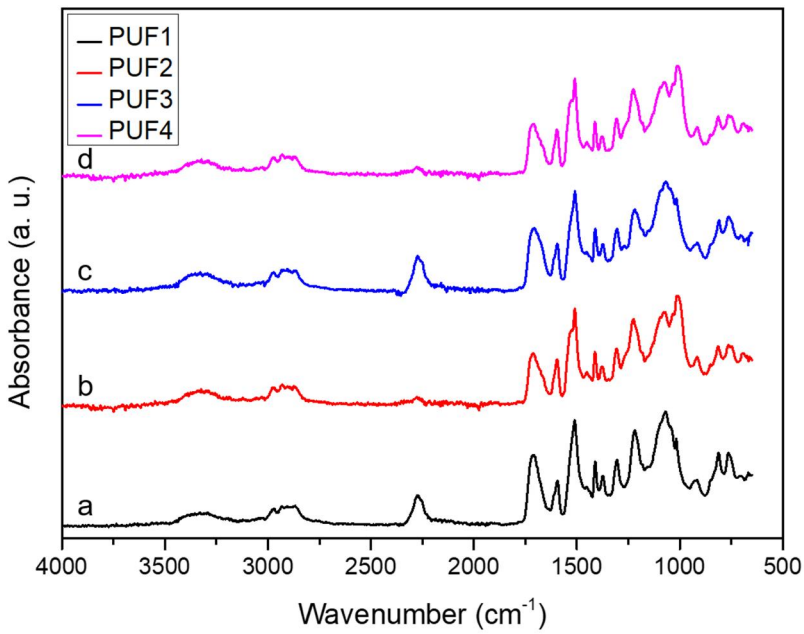

Figure 3.3.4. FTIR spectra of the samples: (a) PUF1, (b) PUF2, (c) PUF3, and (d) PUF4.

3.3.2. Thermal properties

Thermogravimetric analysis (TGA) was carried out under nitrogen or air environment to understand the thermal degradation and thermal oxidation behaviors of the composite foams. The Si-NFCs helped reduce the weight loss of the samples and decompose at relatively high temperature (**Figure 3.3.5**). The thermal stability of the samples increased with increase in the amount of silylation.[76] First, the residual weight of the samples decreased by less than 10% up to 300 ℃. The silylated samples showed larger resistance to the heat than the pristine NFCs in the temperature region under 300 ℃. Namely, the pristine NFCs were dramatically decomposed in the temperature range between 300 and 390℃, but the other samples treated with silylation agent withstood the heat. This was due to the high bonding energy of Si-C and Si-O in the char layer. In the temperature range from 390 to 640 ℃, the residual weight was very different with respect to the amount of silylation (NFC 13%, N1 30.3%, N2 58.3%, N3 65.0%). The char layer generated from silicon elements could prevent the flame propagation effectively and shield the composite material from long burning.

The thermal degradation of the PUFs under nitrogen environment shows three steps (**Figure 3.3.6**). As shown in **Figure 3.3.6a** and **b**, PUF2 and PUF4 showed a decrease in weight at around 200 ℃ due to the thermal degradation of the TCPP. The results indicate that the char forming of PUF4 sample can contribute to flame retardancy although it showed dramatic decomposition between 150℃ and 200℃.[77] The phosphoric acid produced from the TCPP led to the dehydration of polyol and the formation of water from the PUF matrix.[78] The derivative thermogravimetry (DTG) curve of the PUF1 exhibited a sharp drop due to the degradation of polyol and isocyanate structure near 340 ℃.[79] The other samples showed lower weight losses than the PUF1, which was due to the TCPP and Si-NFC. The acidic phosphorus moiety might induce char formation in the samples. The amount of residual char for the PUF3 was 21.0%, which was 2.5 times larger than that of the PUF1 (8.3%). The weight of residual char for the PUF2 and PUF4 increased up to near 17%. These char layer can also protect the polymeric matrix from the flame and impede heat transfer.

The thermal degradation of the PUFs under air atmosphere was considerably different from that under nitrogen environment (**Figure 3.3.6c** and **d**). In the first step, the

TCPP was decomposed at about 190 ℃ and in the second step, the soft segment was decomposed near 330 ℃ [13]. The oxidation of polyol occurred, leading to the degradation to CO_2, water, and urea linkage. In the last step, the hard segment in MDI was decomposed at about 540 ℃. The main difference between in the air and N_2 environments was due to the degradation temperature range of polyol and MDI. The residual char was less than 1% in the case of the PUF1 and 3.5% in the cases of the PUF3 and PUF4. The combination of the TCPP and Si-NFCs could increase the char formation and decrease the mass loss of polymeric structure in PUF1 during the thermal decomposition stage.

The thermal conductivity of PUFs depends on the foam density, cell size, filler contents, ratio of close to open cells, and the thermal conductivity of trapped gases. **Figure 3.3.7** demonstrates the thermal conductivity of the PUFs. When the TCPP was added, the thermal conductivity of the composite PUFs increased due to the deceleration of cell formation. The thermal conductivity of the Si-NFCs was much lower than that of the PUFs in our previous study [22]. As a result of the competition between these different effects, the thermal conductivity of the PUF4 was not significantly changed compared with that of the PUF1.

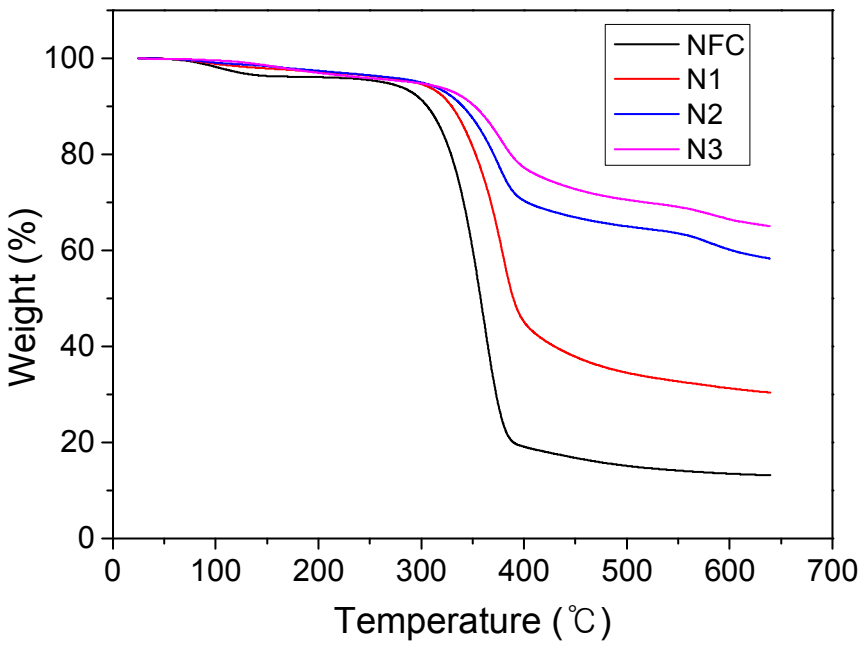

Figure 3.3.5. TGA thermogram of samples in this study: (a) pristine NFC, (b) N1, (c) N2, and (d) N3.

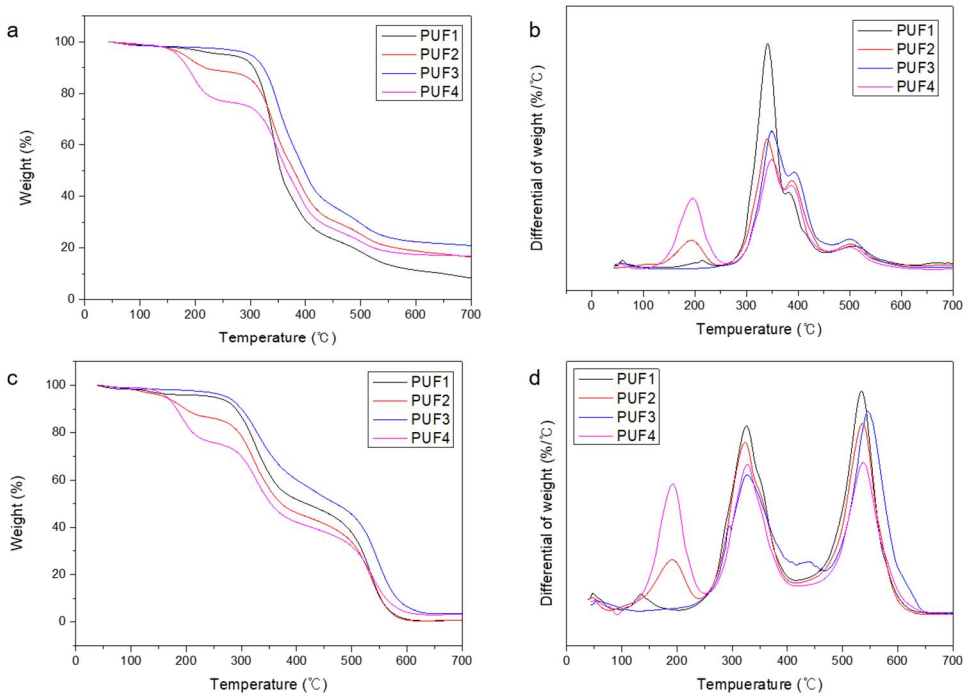

Figure 3.3.6. Thermal stability results of the samples. (a) TGA thermogram and (b) dTGA curve in N_2. (c) TGA thermogram and (d) dTGA curve in air.

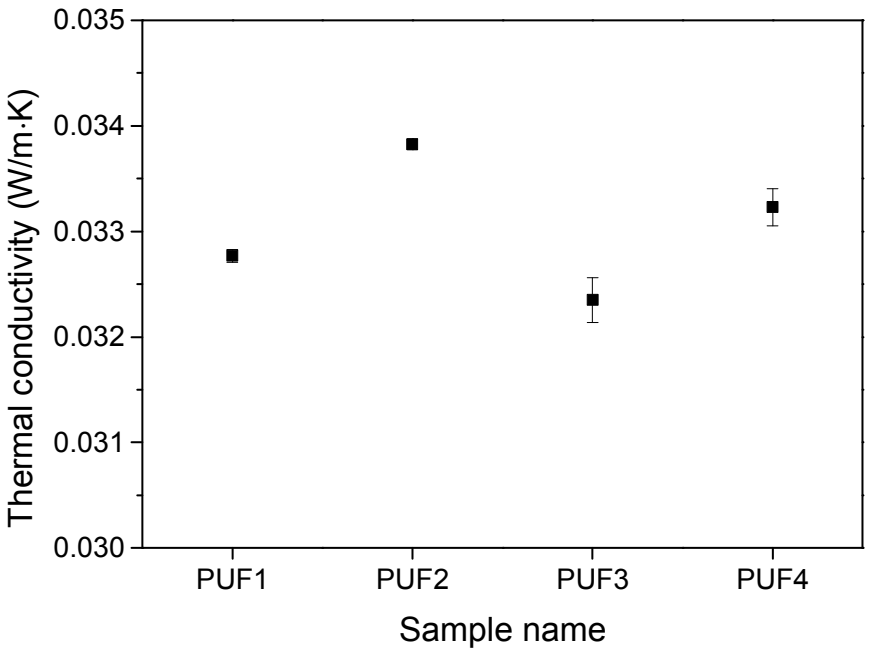

Figure 3.3.7. Thermal conductivity of PUF samples in this study: (a) PUF1, (b) PUF2, (c) PUF2, and (d) PUF3.

3.3.3. Flame retardancy

The flame retardant properties of the PUFs were examined through Limiting Oxygen Index (LOI) and cone calorimeter tests. The higher the LOI value, the better the flame retardancy. **Figure 3.3.8** shows the LOI results of the samples. The PUF1 with the LOI value of 19.3% was burned well in air, and the flame was spread in the environment. The addition of the flame retardant materials increased the LOI values . The LOI of the PUF2 increased to 22.8% by incorporating 20% TCPP. The value of the PUF3 with 5% of Si-NFC was 20.2%, which is not sufficient for self-extinguishment in air. When the TCPP and Si-NFC were loaded together, the LOI of PUF4 increased up to 24.6%, which satisfies the self-extinguishing level.[80]

The cone calorimeter test was carried out to confirm the heat release rate (HRR) and smoke suppression effect of the composite PUFs (**Figure 3.3.9**). The peak of heat release rate (pHRR) is one of the most important parameters since it indicates flashover conditions in real fire condition.[81] In **Figure 3.3.9a**, the pHRR of the PUF1 was 199 kW/m^2, which was not a sufficient value for flame retardancy. When flame came into contact with the surface of the PUF1, black smoke was produced.[82] Incorporating TCPP decreased the pHRR slightly. We tried to add more than 5% of Si-NFC (w/w) to reduce the side effect of the TCPP, but it was hard to process polyurethane foam at higher concentration due to the low density of Si-NFC powder. Although only 5% of Si-NFC was added to the composite foam, the pHRR value was dramatically reduced down to 159 kW/m^2. This can play a crucial role in providing people with time to evacuate from the actual fire catastrophe by delaying fire spread. The PUF4 had the pHRR value of 165 kW/m^2, which was similar to the result of the PUF3.

Smoke production rate (SPR) is also a significant parameter at the fire site since people are more likely to suffer from smoke than flame. Therefore, delaying smoke generation is important in the case of unintentional fire. In general, halogen-based flame retardant materials such as TCPP, which are commonly used in building materials, increase the generation of smoke because they generate radicals to protect the polymeric matrix. The peak of smoke production rate (pSPR) for the PUF2 increased up to 0.118 m^2/s, which was about 30% higher than that of PUF1 (0.089 m^2/s) (**Figure 3.3.9b**)

because gaseous PO and Cl radicals produced by TCPP during the pyrolysis led to the formation of dense smoke. However, the pSPR value decreased to 0.066 m^2/s by adding the Si-NFC. This means that the Si-NFCs in the composite foam efficiently suppressed the side effect of the TCPP.[83] The heat and oxygen barrier generated by the Si-NFCs inhibited the diffusion of smoke during combustion. The PUF4 result indicates that the pSPR of the PUF4 was slightly lower than that of the PUF1.

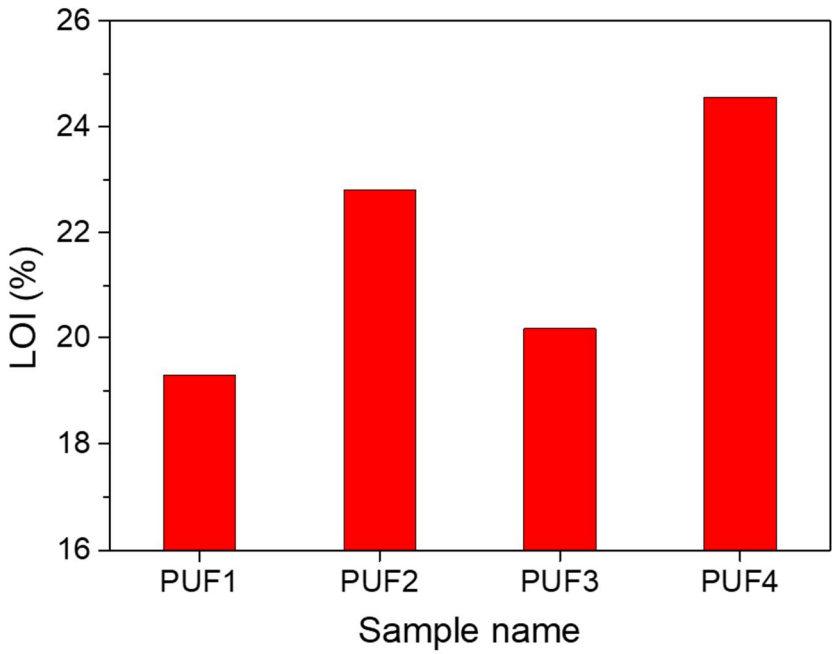

Figure 3.3.8. LOI results of the composite foams.

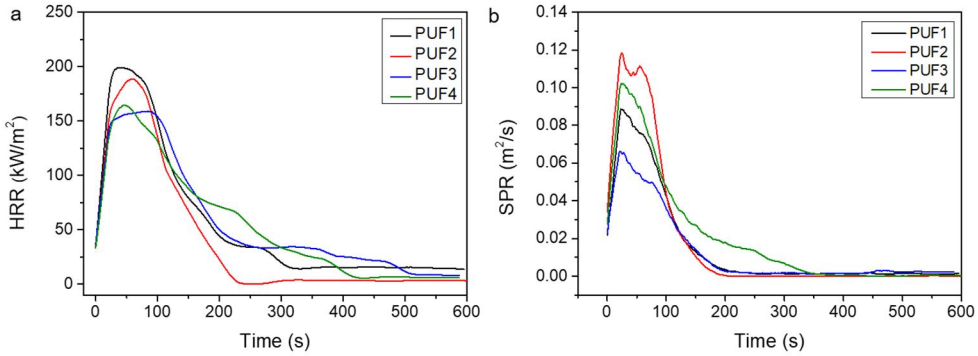

Figure 3.3.9. Results of the cone calorimeter test: (a) heat release rate (HRR) and (b) smoke production rate (SPR).

3.3.4. Residual char analysis

The SEM and EDX analyses of residual char were carried out after the cone calorimeter test to investigate the role of the TCPP and Si-NFCs in the composite PUFs (**Figure 3.3.10**). **Figure 3.3.10a** shows the microscopic images of char of the PUFs. Since the char of PUF1 had a cracked and coarse surface, the char layer could not protect inner polymeric matrix from the outside flame. However, the dense char layer with small cracks and holes was found in the **Figure 3.3.10b**. The holes might be generated due to the strut structure of PUF. The char from the Si-NFCs in the PUF3 showed more rugged structure (**Figure 3.3.10c**). As shown in all the figures, the PUF4 sample had the largest amount of char among the samples (**Figure 3.3.10d**).

EDX analyses were carried out to identify the chemical components of the TCPP and Si-NFC. **Figure 3.3.11** shows the EDX images to confirm the morphology of elements on ash. The ash from the PUF1 consisted of carbon and oxygen atoms (**Figure 3.3.11a**). Since the char was porous, it could not block polymeric matrix from the heat transfer and the flame effectively. The P-O-C bond was formed by the decomposition of the TCPP, which was observed in **Figure 3.3.11b**.[84] On the other hand, it was shown that silicon elements remained unevenly in the residual char of the PUF3 (**Figure 3.3.11c**). The elemental silicon and phosphorus were bonded to the carbon of the residual char and formed the Si-O-Si bond. **Figure 3.3.11d** indicates the good flame retardancy induced by the compact char layer of phosphorus linkage and siliceous char layer, which supports the results of LOI and cone calorimeter.

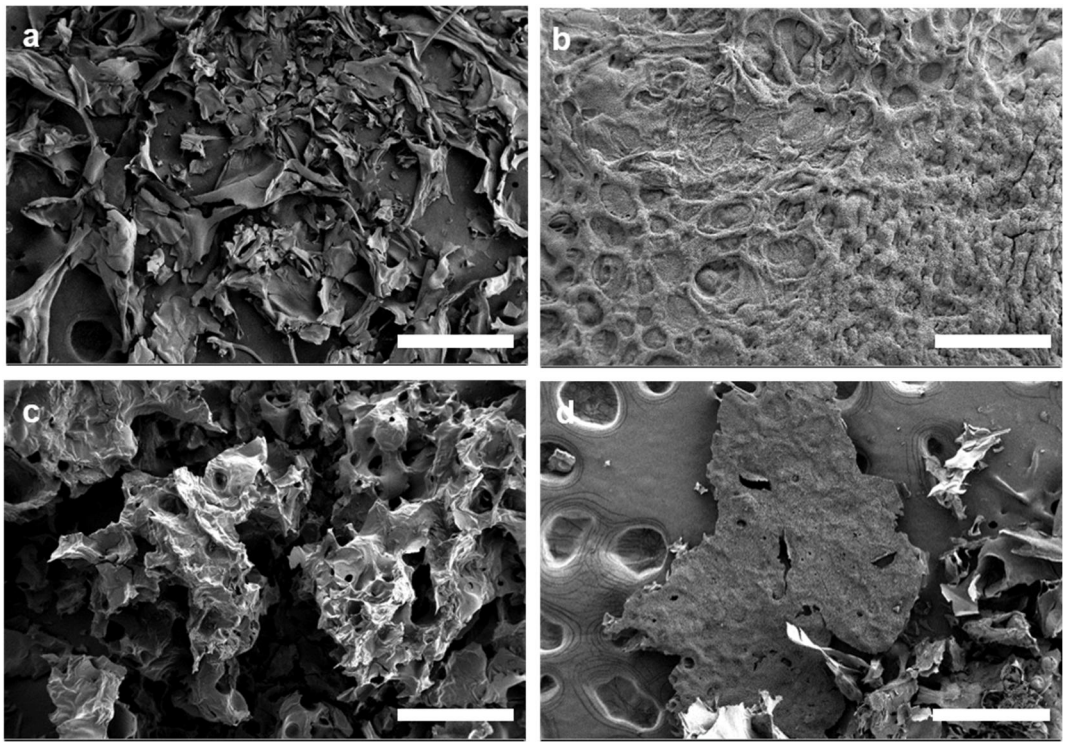

Figure 3.3.10. SEM images of the burned samples: (a) PUF1, (b) PUF2, (c) PUF3, and (d) PUF4 (scale bars : 500 μm).

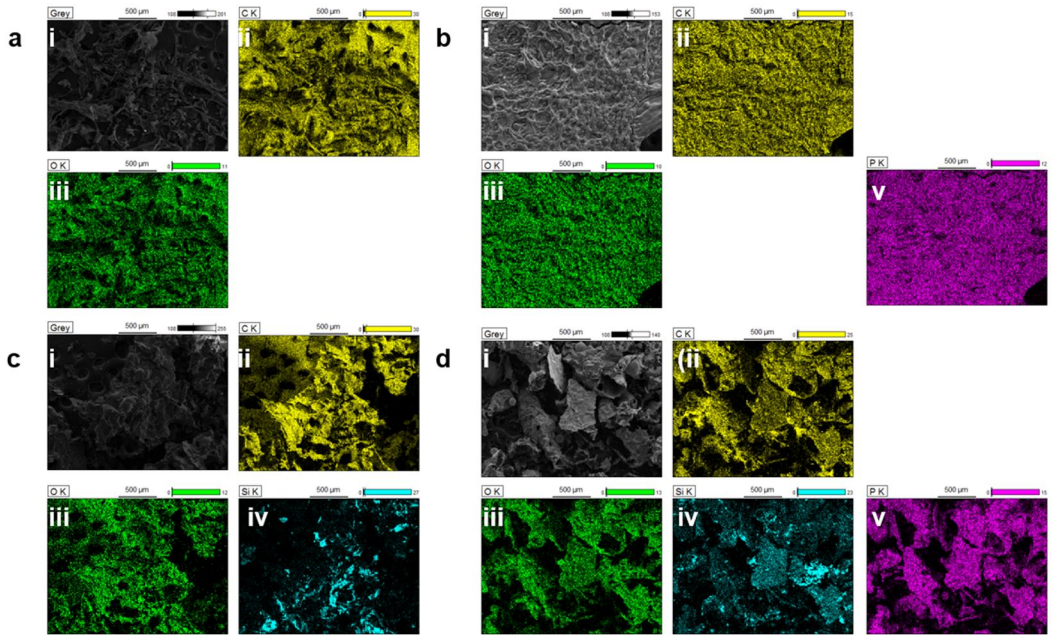

Figure 3.3.11. EDX images of the burned samples: (a) PUF1, (b) PUF2, (c) PUF3, and (d) PUF4. (i) Grey color, (ii) C K line, (iii) O K line, and (iv) Si K line, and (v) P K line (scale bars : 500 μm).

3.4. Conclusions

We fabricated polymeric composite foams by combining a traditional flame retardant, TCPP, and a natural nanoparticle, Si-NFC. The flame retardancy of the polyurethane foam was improved without deteriorating the formability. The thermal stability of the composite foam was enhanced due to the char produced by the Si-O and Si-C bonds. Furthermore, the char protected the polymer matrix from flame by preventing heat transfer. The LOI value of the PUF4 significantly increased from 19.3% to 24.6%, and the incorporation of Si-NFC and TCPP led to decrease in the pHRR and pSPR, which will allow enough time for evacuation in emergency. The EDX and FTIR results confirmed that the phosphorus and silicon elements were bonded to carbon, which produced a dense char layer. We expect that this study will provide a meaningful insight into conventional flame retardant materials and an effective way to increase flame retardancy by using environmentally friendly natural materials.

Chapter IV.

Eco-friendly Nanocellulose Embedded Polymer Composite Foam for Flame Retardancy Improvement

4.1. Introduction

As fire safety has emerged as one of the most important issues in recent years, reliable thermal stability of materials acts as a critical factor in designing building materials, electronics, furniture, textiles, etc.[85] Particularly, flame retardancy, which delays or blocks the flame propagation in the event of a fire, is a momentous characteristic directly related to survival of humans.[86–89]

Flame retardant materials are substances with a sufficiently low flammability causing various physicochemical mechanisms when ignited. Typically, the flame retardant additives are classified into several categories: mineral fillers,[90] hydrate,[91,92] intumescent materials,[93–95] and organohalogen compounds.[96,97] While some retardation mechanisms have been reported such as char formation,[20] gas phase dilution,[98] thermal shielding,[99] endothermic degradation,[100] and gas phase radical quenching,[101] the theoretical exploration still needs to be conducted.[102] Rather than used alone, the flame retardant materials are used as an additive to impart flame retardancy to matrices. For instance, various flame retardants are incorporated into polymeric foams which are widely used for industrial applications such as thermal insulation[103] and sound absorption.[104] However, they have caused a great environmental burden due to the toxicity of the materials themselves.[105] For example, the organohalogen compounds with aromatic rings are thyroid hormone-destroying agents because their chemical structures are similar to hormones.[85] Therefore, development of

materials with high flame retardancy and low toxicity can impose a revolutionary impact to many industries.

A nanocomposite design strategy improves material properties by imparting the pre-eminent properties of nanofillers to the matrix.[106] Among them, nanocellulose is regarded as an attractive filler for composites because of its characteristics such as eco-friendliness,[23] low cost,[41] lightweight,[63] low thermal conductivity,[107] biocompatibility,[39] and facile chemical treatment.[42] In this sense, nanocellulose embedded composites can demonstrate a variety of advantageous material properties. However, the flammability of nanocellulose hinders practical applications as an insulating material. In our previous study,[108] it was reported that chemical functionalization via silylation allows the nanocellulose to possess flame retardancy.[109] When the chemically-treated nanocellulose is burned, carbonized char is generated more actively and delays the flame propagation through the material.[110,111]

In the current study, we developed flame retardant composite foams filled with eco-friendly nanocellulose. When the silylated nanocellulose fibers are embedded in the polyurethane (PU) matrix, the composite foam can provide sufficient flame retardancy with a relatively small amount of conventional flame retardant material. The composite foam also can maintain mechanical and thermal insulation properties, which are normally degenerated by the addition of conventional flame retardant materials. The characteristics of the samples were investigated to understand the enhancement mechanisms.

4.2. Experimental

4.2.1. Preparation of flame retardant nanocellulose.

nanofibrillated celluloses (NFCs), also called nanofibrilated celluloses, were purchased from University of Maine – Process Development Center (United States). Before the usage, NFCs were dispersed in water by stirring for 24 hours, ultrasonicated 30 minutes, and lyophilized in a bid to separate them. The silylation process for imparting flame retardancy to NFCs was performed using MTMS (Methyltrimethoxysilane, 97%, Alfa Aesar, United States). Depending on the mass ratio of NFC and MTMS, three silylated NFC samples were prepared, which were denoted as silylated nanofibrilated celluloses (Si-NFCs) 1 (NFCs:MTMS=1:1), Si-NFCs 2 (1:3), and Si-NFCs 3 (1:5). In this study, the Si-NFCs 3 was selected as an additive embedding in the composite foams because of its good flame retardancy verified in our previous work.[66] The 5 wt% MTMS/water solution was added dropwise to the 1% NFCs/water solution. The chemical reaction was carried out under aqueous condition while stirring for 130 minutes. After completion of the reaction, the NFCs/MTMS/water solution was poured into a conical tube and lyophilized to obtain a dried powder of the Si-NFCs samples.

4.2.2. Fabrication of flame retardant foam.

A polyether polyol mixture (MCNS Rigid System Polyol, Mitsui Chemicals & SKC Polyurethanes Inc., Republic of Korea) and polymethylene polyphenyl isocyanate (COSMONATE M-200, Mitsui Chemicals & SKC Polyurethanes Inc., Republic of Korea) were employed as base chemical resins for fabricating polyurethane (PU) foams. 3 wt% of water was added to the polyol mixture as a chemical blowing agent. The two resins were mixed vigorously at 3000 rpm with a 1:1.3 mass ratio of the polyol resin and the isocyanate resin. The mixed resin was poured into an acrylic mold with the dimension of 10 cm × 10 cm × 5 cm. The amount of poured resin was adjusted to produce a foam of 50 kg/m^3 density. The surface of the mold was coated with a demolding agent, AKO-HM207K (Akochem, Republic of Korea). Temperature of the mold was maintained at 60℃ through the foaming reaction. Three different flame retardant foams were fabricated: (i) foam containing only a conventional flame retardant (polyurethane foam/Tris(2-chloroethyl) phosphate, PUF/TCEP), (ii) foam containing only Si-NFCs (PUF/Si-NFCs), and (iii) foam containing both flame retardants (PUF/Si-NFCs/TCEP). 20 wt% of Tris(2-chloroethyl) phosphate (TCEP, Sigma Aldrich, United States), a conventional flame retardant, was added into the polyol mixture. The flame retardant PU composite foams were filled with 5 wt% of the Si-NFCs after the polyol/Si-NFCs was vigorously mixed at 3000 rpm. The PUF/Si-NFCs/TCEP sample was prepared by adding both flame retardants into the polyol mixture. The remaining manufacturing processes were the same as the PU foaming process described above.

4.2.3. Characterizations.

Microstructure morphology of the fabricated samples was observed using a field-emission scanning electron microscope (FE-SEM, MERLIN Compact, ZEISS, Germany). The aqueous solution containing NFCs was dropped onto a silicon wafer, and the water was dried. The foam samples were cut into specimens after freeze-drying with liquid nitrogen to preserve the microcellular structures. The prepared specimens were coated with Pt using a sputter (MSC-101, JEOL, Germany). Energy-dispersive X-ray spectroscopy (EDX) equipped with the FE-SEM was used for the chemical element analysis of the specimens. To investigate the chemical structures of the samples, Fourier transform infrared spectroscopy (Cary 660 FTIR Spectrometer, Agilent, United States) was employed with the Varian Resolutions Pro software. All data were obtained at a resolution of 4 cm^{-1} from 4000 cm^{-1} to 650 cm^{-1}. The acquired data were normalized as an arbitrary unit from zero to one to compare the intensities directly. Thermal stability of the samples was examined using a thermogravimetric analyzer (SDT Q600, TA Instruments, Australia). The samples were heated from room temperature to 600°C at a heating rate of 20°C/min under a nitrogen flow of 100 ml/min. The thermal conductivity of the samples was measured by using a thermal analyzer (C-Therm TCi, C-Therm Technologies Ltd, New Brunswick, Canada). Limiting oxygen index (LOI), a standard of flame retardancy was measured by using a flammability tester based on ASTM D2863/77 (Stanton Redcroft, United Kingdom). Mechanical properties of the foam samples were investigated using a universal testing machine (UTM, WL2100, WITHLAB, Republic of Korea) with a clamp for the compression mode. A cone calorimeter (Cone Calorimeter ISO 5660, Festec International Co. Ltd., Republic of Korea) was used to measure the heat release rate, smoke release, ignition time, oxygen consumption, carbon monoxide and carbon dioxide generation, and mass loss rate. All the prepared samples were conditioned at room temperature and 50% relative humidity for at least 7 days before testing to satisfy equilibrium conditions. A constant irradiation heat flux of 50 kW/m^2 was irradiated to the testing samples while opening the thermal shutter, and an electric spark was used for ignition. The samples were tested more than twice to validate repeatability.

4.3. Results and discussion

4.3.1. Characterizations. Fabrication of PU composite foam.

The composite foams with enhanced flame retardancy were made by incorporating flame retardant nanocellulose fillers and a conventional flame retardant, Tris(2-chloroethyl) phosphate (TCEP) into PU foam. We experimentally set the filler contents since TCEP of 20 wt% or more and NFCs of 5 wt% or more affected to dimensional stability of foams. Prior to the fabrication, the flame retardant nanocellulose is prepared through the chemical treatment of silylation. The cellulose nanofibers (NFCs) were prepared by using the same chemical treatment as our previous work employing silylated cellulose nanocrystal (NCC).[66] In this study, NFCs were chosen since they have several advantages over NCC, such as low thermal conductivity, eco-friendliness, and ease of chemical treatment. The surface of treated NFCs were covered with polysiloxane layers as demonstrated in **Figure 4.3.1a** and **b**. The sample was named as silylated nanofibrilated celluloses (Si-NFCs). The chemical treatment can enhance the amount of generated chars during burning. The polyurethane foams (PUFs) were fabricated using foam reaction molding method where polyol and isocynate resins are mixed vigorously and poured into a mold for curing. We fabricated four different samples: neat PUF, PUF/Si-NFCs, PUF/TCEP, and PUF/Si-NFCs/TCEP as shown in **Figure 4.3.2**. Details about the method are described in the experimental section.

The microcellular structure of the composite foam was observed with an FE-SEM (field emission scanning electron microscope) (**Figure 4.3.3**). The average cell diameter of the neat PUF was 416.9±55.6 μm (**Figure 4.3.3a**). The critical energy required for nucleation can be lowered significantly on the surface of the nano-size particles.[112] Therefore, the presence of the Si-NFCs in the resin mixture provoked uniform microcellular distribution in the PUF during foaming reaction, resulting in a mean cell diameter of 266.5±68.7 μm (**Figure 4.3.3b**). On the contrary, TCEP increased the cell size (i.e., the average cell diameter of 488.3±82.3 μm, **Figure 4.3.3c**), since it reacted with the cyanate groups of the resin and changed the balance between the foaming and the gelling reactions. This phenomenon weakens the mechanical stiffness of

the foam samples, which is why TCEP is not generally used for flame retardancy as a single additive. Moreover, the PU resin and TCEP mixture has low blowing rate during foaming reaction, resulting in poor formability. On the other hand, the combination of Si-NFCs and TCEP increased the cell nucleation rate as shown in **Figure 4.3.3d** (the average cell diameter, 327.6±76.4 μm). Since the Si-NFCs increased the viscosity of the resin mixture during foaming reaction, the growth of microcells were more stable. In addition, increase in the nucleation rate due to the nanocellulose fillers led to good formability.

Chemical structure of the samples was investigated using the FTIR (Fourier-transform infrared spectroscopy) spectra (**Figure 4.3.4**). In the neat PUF FTIR spectra, the broad peak near 3400 cm^{-1} indicates hydroxyl moieties on the molecular chain of the polyol-based resin. The peak at 1708 cm^{-1} corresponds to the C=O bond in the ester moiety (RCOOR') of the polyol-based resin and urethane linkage moiety (R–NHCOO–R'). The urea linkage peak is shown at 1412 cm^{-1}, indicating the gelling reaction between hydroxyl groups and cyanate groups.[113] The peaks found at 2970 cm^{-1}, 2872 cm^{-1}, 1595 cm^{-1}, and 1073 cm^{-1} are due to CH_3 vibration, CH_2 vibration, aromatic ring, and C-O bond, respectively.[39,40] For the samples containing Si-NFCs, a slightly overlapped broad absorption peak in the 1000–1100 cm^{-1} region is discovered due to the Si–O–Si bonds by silylation. The FTIR peak of the Si-C bond is observed at 762 cm^{-1}. On the other hand, the phosphorus related peaks at 1308 cm^{-1} and 1015 cm^{-1} indicating P=O and P-O-C bonds were found in the samples incorporating TCEP, the PUF/TCEP and PUF/Si-NFCs/TCEP. From the FTIR analysis, it was verified that the overall chemical structure of the embedded chemicals and fillers are preserved without undesired modifications.

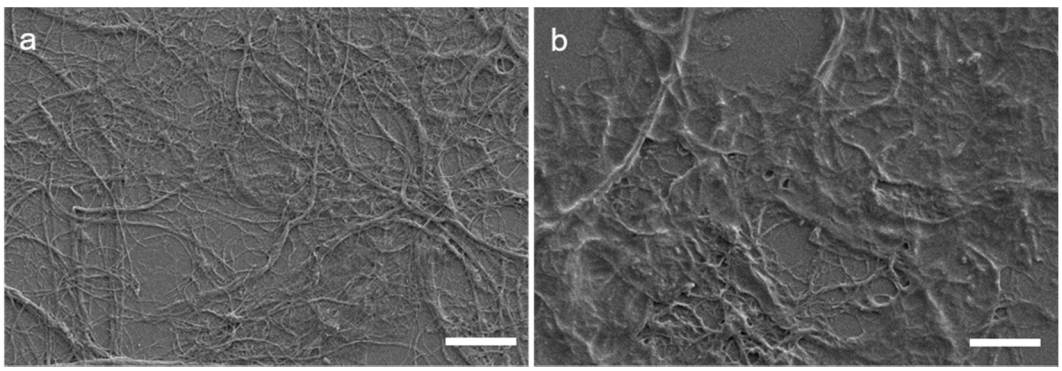

Figure 4.3.1. Morphology of (a) the neat NFCs and (b) the silylated NFCs (Si-NFCs) (Scale bars : 2 μm).

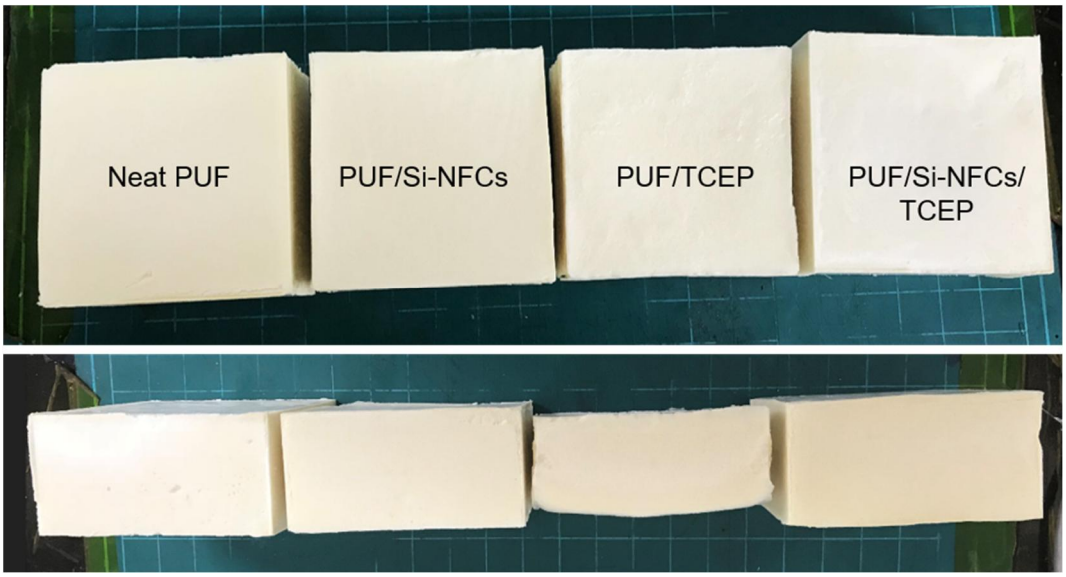

Figure 4.3.2. Optical photographs of the fabricated foams.

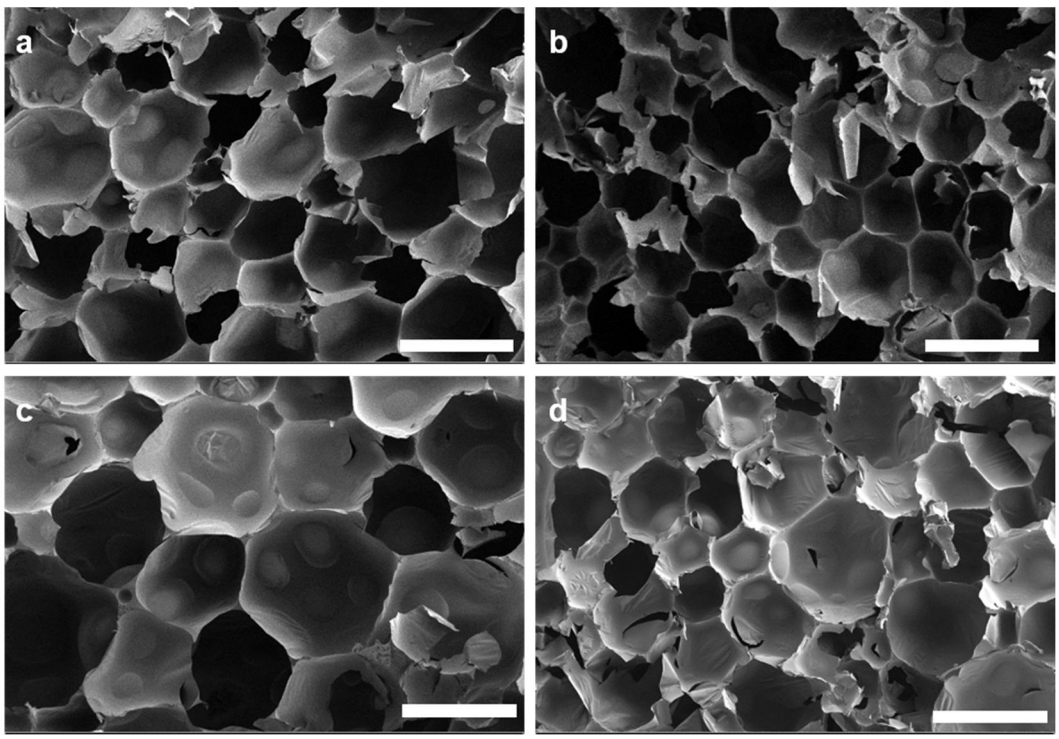

Figure 4.3.3. Microcellular structures of the fabricated foams for (a) the neat PUF, (b) the PUF/Si-NFCs, (c) the PUF/TCEP, and (d) the PUF/Si-NFCs/TCEP samples.

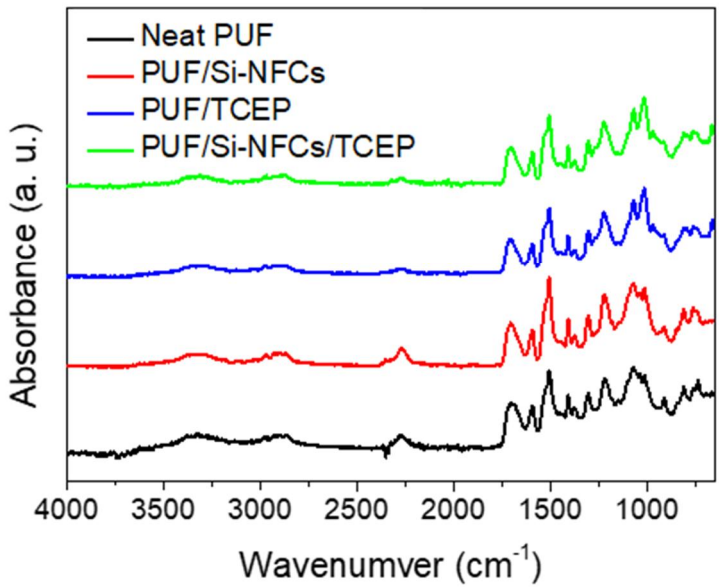

Figure 4.3.4. FTIR spectra of the samples.

4.3.2. Thermal and mechanical properties.

Thermal stability of the samples was examined through TGA (thermogravimetric analysis) (**Figure 4.3.5a, b**). The thermal stability of the neat PUF was improved by adding the Si-NFCs. The final residue after heating the samples up to 700℃ (3.7 wt%) was increased by 2.8 times compared with the PUF/Si-NFCs sample (10.5 wt%). Since the thermal conductivity of Si-NFC is lower than that of polyurethane matrix, embedding the Si-NFCs can enhance the thermal stability of the PUF. Furthermore, our previous study reported that the silylation treatment of NFCs enhanced the thermal stability.[66] Incorporation of TCEP into the PU matrix similarly increased the residual char at the final temperature of 700℃ (12.2 wt%) and lowered the thermal stability of the PUF compared with the neat PUF in the temperature range from 200 to 400℃. The TCEP molecules were thermally decomposed at the relatively low temperature range due to the generation of P-O-C and P-C to form phosphinic acid before the collapse of PU chains. This might have adverse effects on thermal stability of the PUF, but the residue of the PUF/TCEP sample increased by about 1.5 times compared with that of the neat PUF when heated up to 700℃. Its major mechanism is explained by the formation of carbonized layer after rapid thermal decomposition, which blocks heat transfer from the outside and facilitates char formation. The residual char of the PUF/Si-NFCs/TCEP sample was improved synergistically, which is larger than that of the neat PUF sample by about 5 times when heated up to 700℃. This is a meaningful result for industrial applications since the thermal stability of the material is important in the event of a fire. **Figure 4.3.5b** shows the differential curves of the TGA thermograms for the four samples.

Mechanical stiffness of the samples was measured by using a UTM (universal test machine) in a compression mode, and the results were compared as shown in **Figure 4.3.6**. The compressive stress-strain (S-S) curve of the neat PUF was compared with the curve of the PUF/Si-NFCs. It is well known that nanoscale fillers reinforce the matrix material due to their exceptional aspect ratio and large surface area. Although the silylation treatment on NFCs might reduce the mechanical properties compared with the use of pristine NFCs, the elastic modulus of the PUF/Si-NFCs (25.0 MPa) is greater than that of the neat PUF (17.1 MPa) by 1.5 times. On the contrary, the addition of TCEP into PUF lowered the elastic modulus of the foam by 1.7 times (10.0 MPa). It is presumed that

the TCEP intercalated in the resin hinders the gelling reaction between –OH and -NCO and deteriorates the stiffness of the PUF. Accordingly, the molecular weight of the resin was lowered. Adopting both Si-NFCs and TCEP compensated this shortcoming and improved the mechanical property of the composite foams by achieving the elastic modulus of 12.1 MPa for the PUF/Si-NFCs/TCEP sample.

Thermal conductivity is one of the most important properties of building materials such as PUF. Many studies have been conducted to improve the thermal insulation performance of porous materials by tuning microcellular structures while other macroscopic properties remain unchanged.[114,115] The thermal conductivity of the neat PUF was 33.6 mW/m·K, which is a typical value for conventional PU foams (**Figure 4.3.7**). Embedding Si-NFCs in the PUF decreased the thermal conductivity slightly. This decrease in thermal conductivity can be explained by two mechanisms; structural change to smaller and more uniform cell size distribution (**Figure 4.3.3b**) and altered material composition. The foams with small microcellular sizes have been reported to show good thermal insulation,[116] and furthermore, thermal conductivity of the cellulose material itself is slightly lower than that of PU matrix.[117] Meanwhile, TCEP induces relatively large and non-uniform microcells (**Figure 4.3.3c**), which resulted in poor thermal insulation. It was found that the insulation property of the PUF/Si-NFCs/TCEP sample is similar to that of the neat PUF (**Figure 4.3.3d** and **Figure 4.3.7**).

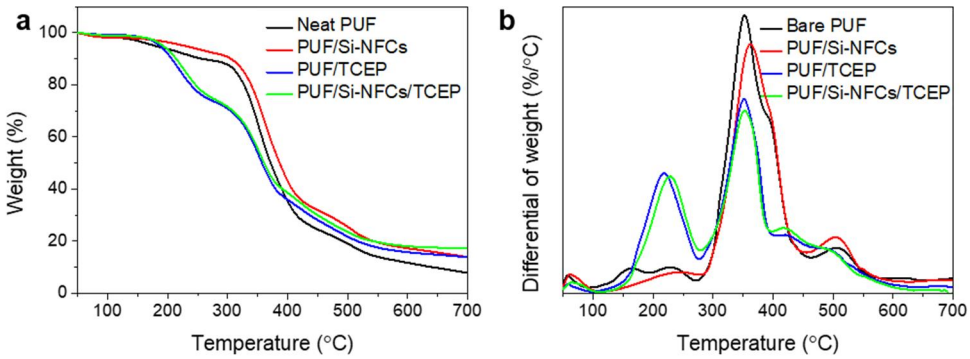

Figure 4.3.5. Thermal and mechanical properties of the fabricated composite foams. (a) TGA thermogram, (b) DTGA.

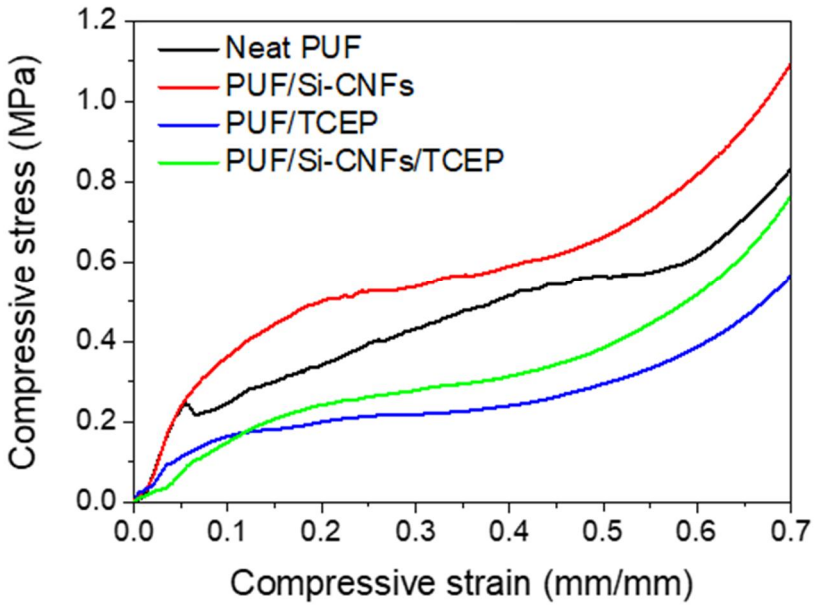

Figure 4.3.6. Compressive stress-strain curves.

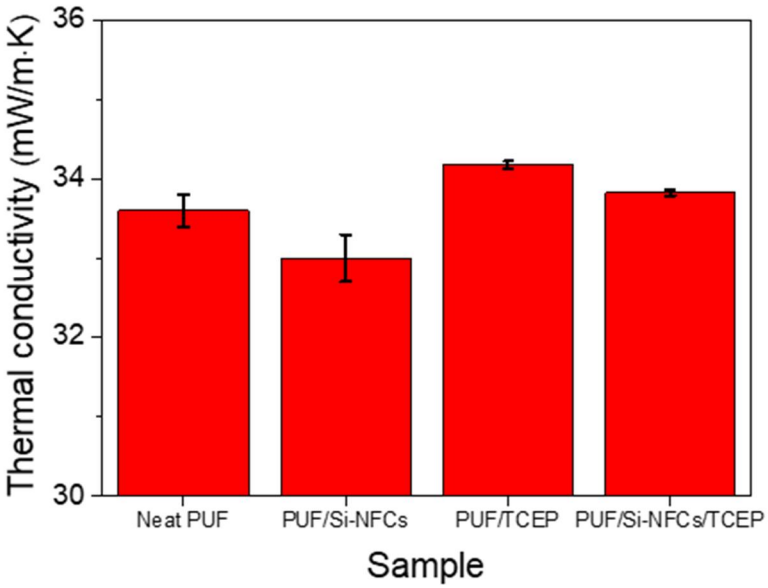

Figure 4.3.7. Thermal conductivities of the samples.

4.3.3. Flame retardancy test.

Flame retardancy was investigated by conducting a low oxygen index (LOI) test (**Figure 4.3.8a** and **b**). **Figure 4.3.3a** shows how to measure the LOI value. The LOI value of the neat PUF was about 21%, which is the typical value of porous polymers. Since atmospheric oxygen concentration is the same as the LOI value of the neat PUF (about 21%), fire on the PUF is not extinguished easily.

NFC is a combustible material which is not used as a flame retardant because it contains hydrocarbon chains. However, the silylation treatment of NFC converted this combustible material into a flame retardant material by increasing the production rate of char during combustion due to the generated Si-O and Si-C groups on NFCs. (e.g., the LOI value of around 35%).[34] Incorporating Si-NFCs into the matrix increased the LOI up to 22%. Since the value is larger than the atmospheric oxygen concentration. It is expected that larger amount of Si-NFCs in polymer matrix would offer better flame retardancy. However, this expectation was not verified experimentally because the resin viscosity increased dramatically when more than 5 wt% Si-NFCs were added to the polyol-based resin. When the LOI test was conducted for the neat PUF sample, color of the smoke was deep-black, which indicates incomplete combustion. Under the presence of Si-NFCs in the PUF, the reaction balance between the PU combustion and supply of oxygen is changed by generating Si-C and Si-O bonds, and then the smoke color became white upon burning.

On the other hand, the TCEP chemical is one of the most frequently used flame retardant due to its outstanding performance. Phosphate atoms of TCEP can hinder the transfer of reactive radicals to polymeric chains and then prevent the propagation of flames into the material. As expected, the PUF/TCEP showed a superior flame retardancy, the LOI value of 25%. Despite this good performance, the use of TCEP is strongly sublated due to environmental problems and health hazards, which are caused by the extremely toxic gases generated during combustion. In this sense, we fabricated hybrid composite foams by combining Si-NFCs with TCEP. Interestingly, the LOI value of the PUF/Si-NFCs/TCEP composite foam was measured as over 28%, which is higher than the weighted mean of LOI values of the two additives. This synergistic effect was realized

by the rapid char formation and the protection of polymeric chains through blocking the radical transfer at the same time in the PU matrix upon burning.

The heat release rate (HRR) and smoke production rate (SPR) of the samples were measured by the cone calorimeter to investigate the physics of combustion (**Figure 4.3.9a, b**). The HRR value implies the rate of heat generation upon fire indicates the flammability, which is proportional to the oxygen consummation. The total heat released through burning is the same for the samples because of the same calorific value for each sample upon fire. The peaks of HRR values of the neat PUF, PUF/Si-NFCs, PUF/TCEP, PUF/Si-NFCs/TCEP samples were varied from 156 kW/m^2, 122 kW/m^2, 95 kW/m^2, to 78 kW/m^2, respectively. A low HRR value means that the propagation speed of heat along the external flame is slow. Compared with the neat PUF, the PUF/Si-NFCs/TCEP had a half HRR value due to the synergistic effect. On the other hand, the SPR value is a measure of the rate of generation of toxic gases during combustion that can pose a threat to life and environment.[118] The presence of TCEP in the PU foam accelerated the smoke generation, which is the emission of radical from the burnt TCEP (**Figure 4.3.9b**). The Si-NFCs lowered the peak of smoke production rate (SPR) value of the PUF/Si-NFCs/TCEP sample to the PUF/TCEP level. In this way, Si-NFC can help flame retardancy of TCEP.

The structural features of the ash remaining after burning were observed to account for the improved flame retardancy from a different perspective. The macroscopic images of the burned samples were demonstrated in **Figure 4.3.10**. Compared with the samples without Si-NFCs, other samples showed a relatively high structural stability after the cone calorimeter test. The formation of a siliceous char by Si-NFCs maintained the morphological dimension of the samples unlike the neat PUF. Also, the fired PUF/TCEP and PUF/Si-NFCs/TCEP samples were formed with the intumescent char layers.[119] This characteristic is useful for designing a fire safe building because the collapse time of buildings can be delayed by blocking flame. This improved structural robustness can be understood by assessing the microstructures of the samples (**Figure 4.3.11a-d**). From the SEM images of the samples with Si-NFCs, the sample surfaces were entirely covered with a rigid-looking layer consisting of char, Si-C, and SiO_2. The EDX images revealed that the flame retardancy of the foam composite was affected considerably by the

existence of silicon atoms (Si-C and SiO_2) although Si-NFCs were agglomerated in the sample surfaces. Meanwhile, the neat PUF and PUF/TCEP samples were wrapped by a porous layer without Si. The phosphorus atoms were evenly located on the entire surface of the samples with TCEP. The uniform distribution of phosphorus element on the surface ensured better flame retardancy by producing intumescent char layers formed by the bonds of P=O and P-O-C. Consequently, the synergistic effect of flame retardation was confirmed by the structural stability due to the formation of rigid char layers and the lagging of radical propagation rate inside the polymer backbone.

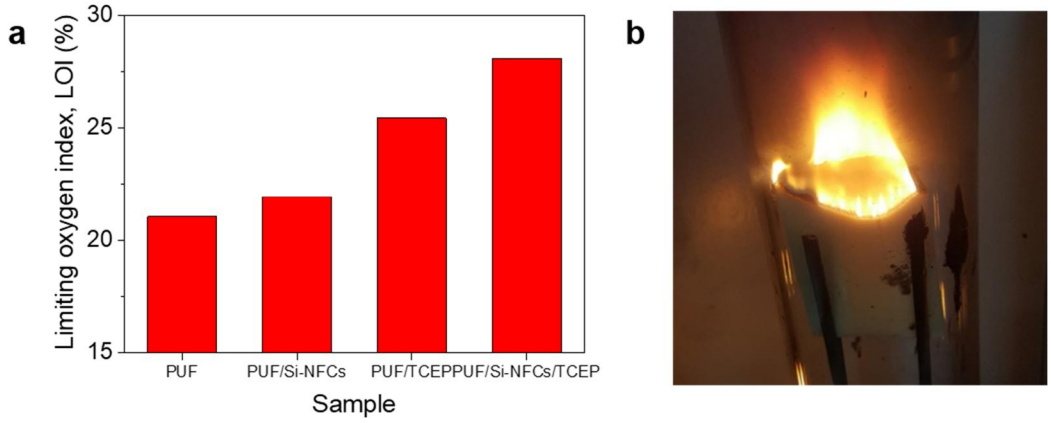

Figure 4.3.8. Flame retardancy of the synergetic composite foams. (a) Limiting oxygen index (LOI) results of the fabricated foams and (b) the photograph of the LOI test.

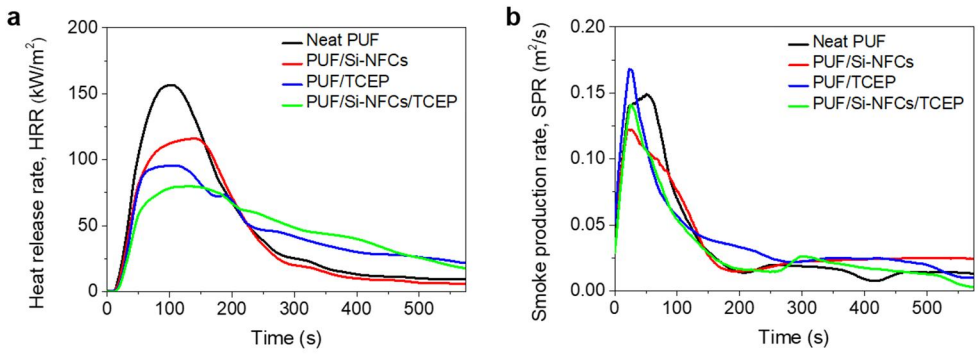

Figure 4.3.9. (a) time-dependent heat release rate (HRR), and (b) smoke production rate (SPR) of the samples while burning in the cone calorimetry.

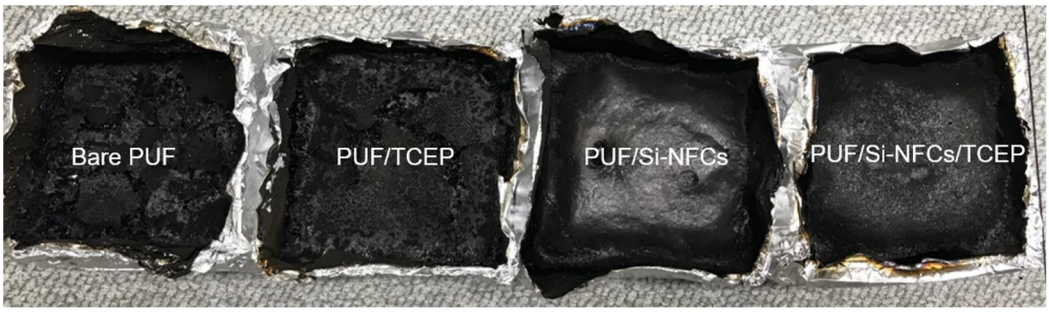

Figure 4.3.10. Macro/microscopic analyses of the burned samples. Macroscopic pictures after burning (Sample sizes : 10 cm).

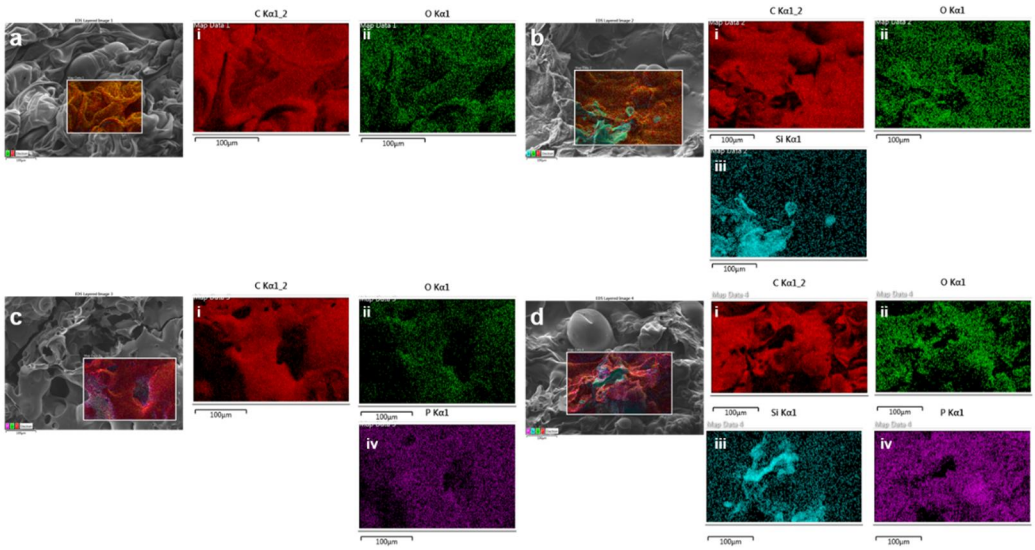

Figure 4.3.11 EDX data of (a) the neat PUF, (b) PUF/Si-NFCs, (c) PUF/TCEP, and (d) PUF/Si-NFCs/TCEP samples after burning. Each right sub-figure displays (i) C K line, (ii) O K line, (iii) Si K line, and (iv) P K line. The error bar indicates 100 μm.

4.4. Conclusions

In this study, we fabricated a flame retardant polyurethane composite foam incorporated with Si-NFCs. Addition of Si-NFCs into the PUF led to the reduction in cell size and the homogenous microcellular structure by accelerating the rate of cell nucleation in the PU matrix. This structural advantage prevented the deterioration of the mechanical strength and thermal insulation. Combining Si-NFCs with TCEP opens a way to obtain high flame retardancy, i.e., the high LOI value of 29%, while reducing existing flame retardant agent. In addition, Si-NFCs increased the moldability of the PU resin containing TCEP. In the cone calorimetry test, low HRR and SPR values were obtained for the PUF/Si-NFCs/TCEP sample, implying both high flame retardancy and relatively lowered environmental burden. The membrane covering the burned sample surface was structurally investigated. The strategy proposed in this study will provide a way for reducing environmental burden of insulating materials and improving flame retardant performance.

Chapter V.

Concluding Remarks

Nanocellulose can be obtained by acid treatment, fibrillization, etc., and is one of natural polymers present in nature. Cellulose is a combustible material, but it has been chemically modified to silanize it. The polysiloxane layers formed on the surface gives flame retardancy. Using a NCC, it is possible to produce nanocellulose having a very high LOI value and low thermal conductivity. In a similar method, fibrillated cellulose was prepared and put into a polyurethane foam together with a commercial flame retardant such as TCPP or TCEP. As a result, the heat release rate and smoke generation rate were reduced and the LOI value also increased. Particularly, it was confirmed that the cell size was not increased even though the silylated nanocellulose had the flame retardant, and the phenomenon of the foaming was not inhibited by the flame retardant agent. Since these polymer composite materials have the same flame retardancy as conventional ones but use environmentally friendly fillers, a method of reducing the amount of harmful flame retardant is proposed.

Bibliography

[1] Y. Ogasawara, S. Itagaki, K. Yamaguchi, N. Mizuno, Saccharification of natural lignocellulose biomass and polysaccharides by highly negatively charged heteropolyacids in concentrated aqueous solution, ChemSusChem. 4 (2011) 519–525. doi:10.1002/cssc.201100025.

[2] N. Lin, C. Bruzzese, A. Dufresne, TEMPO-oxidized nanocellulose participating as crosslinking aid for alginate-based sponges, ACS Appl. Mater. Interfaces. 4 (2012) 4948–4959. doi:10.1021/am301325r.

[3] D. Bondeson, A. Mathew, K. Oksman, Optimization of the isolation of nanocrystals from microcrystalline cellulose by acid hydrolysis, Cellulose. 13 (2006) 171–180. doi:10.1007/s10570-006-9061-4.

[4] P.B. Filson, B.E. Dawson-Andoh, Sono-chemical preparation of cellulose nanocrystals from lignocellulose derived materials, Bioresour. Technol. 100 (2009) 2259–2264. doi:10.1016/j.biortech.2008.09.062.

[5] A.M. Salaberria, S.C.M. Fernandes, R.H. Diaz, J. Labidi, Processing of α-chitin nanofibers by dynamic high pressure homogenization: Characterization and antifungal activity against A. niger, Carbohydr. Polym. 116 (2015) 286–291. doi:10.1016/j.carbpol.2014.04.047.

[6] I. Besbes, S. Alila, S. Boufi, Nanofibrillated cellulose from TEMPO-oxidized eucalyptus fibres: Effect of the carboxyl content, Carbohydr. Polym. 84 (2011) 975–983. doi:10.1016/j.carbpol.2010.12.052.

[7] S.P. Lin, I. Loira Calvar, J.M. Catchmark, J.R. Liu, A. Demirci, K.C. Cheng, Biosynthesis, production and applications of bacterial cellulose, Cellulose. 20 (2013) 2191–2219. doi:10.1007/s10570-013-9994-3.

[8] S.M. Keshk, Bacterial Cellulose Production and its Industrial Applications, J. Bioprocess. Biotech. 04 (2014). doi:10.4172/2155-9821.1000150.

[9] L. Hu, G. Zheng, J. Yao, N. Liu, B. Weil, M. Eskilsson, E. Karabulut, Z. Ruan, S. Fan, J.T. Bloking, M.D. McGehee, L. Wågberg, Y. Cui, Transparent and conductive paper from nanocellulose fibers, Energy Environ. Sci. 6 (2013) 513–518. doi:10.1039/c2ee23635d.

[10] Y.H. Jung, T.H. Chang, H. Zhang, C. Yao, Q. Zheng, V.W. Yang, H. Mi, M. Kim, S.J. Cho, D.W. Park, H. Jiang, J. Lee, Y. Qiu, W. Zhou, Z. Cai, S. Gong, Z. Ma, High-performance green flexible electronics based on biodegradable cellulose nanofibril paper, Nat. Commun. 6 (2015) 1–11. doi:10.1038/ncomms8170.

[11] S. Kalia, A. Dufresne, B.M. Cherian, B.S. Kaith, L. Avérous, J. Njuguna, E. Nassiopoulos, Cellulose-based bio- and nanocomposites: A review, Int. J. Polym. Sci. 2011 (2011). doi:10.1155/2011/837875.

[12] G. Hayase, K. Kanamori, K. Abe, H. Yano, A. Maeno, H. Kaji, K. Nakanishi, Polymethylsilsesquioxane-cellulose nanofiber biocomposite aerogels with high thermal insulation, bendability, and superhydrophobicity, ACS Appl. Mater. Interfaces. 6 (2014) 9466–9471. doi:10.1021/am501822y.

[13] H.B. Zhao, M. Chen, H.B. Chen, Thermally Insulating and Flame-Retardant Polyaniline/Pectin Aerogels, ACS Sustain. Chem. Eng. 5 (2017) 7012–7019. doi:10.1021/acssuschemeng.7b01247.

[14] A.M. Papadopoulos, State of the art in thermal insulation materials and aims for future developments, Energy Build. 37 (2005) 77–86. doi:10.1016/j.enbuild.2004.05.006.

[15] S.K. Brown, Penetration Wetting of Asbestos Insulation Products, Ind. Eng. Chem. Res. 29 (1990) 2123–2128. doi:10.1021/ie00106a023.

[16] J. Cai, S. Liu, J. Feng, S. Kimura, M. Wada, S. Kuga, L. Zhang, Cellulose-silica nanocomposite aerogels by in-situ formation of silica in cellulose gel, Angew. Chemie - Int. Ed. 51 (2012) 2076–2079. doi:10.1002/anie.201105730.

[17] K. Ghazi Wakili, R. Bundi, B. Binder, Effective thermal conductivity of vacuum insulation panels, Build. Res. Inf. 32 (2004) 293–299. doi:10.1080/0961321042000189644.

[18] X. Chen, L. Huo, J. Liu, C. Jiao, S. Li, Y. Qian, Combustion properties and pyrolysis kinetics of flame-retardant polyurethane elastomers, J. Thermoplast. Compos. Mater. 30 (2017) 255–272. doi:10.1177/0892705715598361.

[19] E. Jakab, M.A. Uddin, T. Bhaskar, Y. Sakata, Thermal decomposition of flame-retarded high-impact polystyrene, in: J. Anal. Appl. Pyrolysis, (2003) 83–99. doi:10.1016/S0165-2370(03)00075-5.

[20] J.H. Cho, V. Vasagar, K. Shanmuganathan, A.R. Jones, S. Nazarenko, C.J. Ellison, Bioinspired Catecholic Flame Retardant Nanocoating for Flexible Polyurethane Foams, Chem. Mater. 27 (2015) 6784–6790. doi:10.1021/acs.chemmater.5b03013.

[21] N.T. Cervin, L. Andersson, J.B.S. Ng, P. Olin, L. Bergström, L. Waìšgberg, Lightweight and strong cellulose materials made from aqueous foams stabilized by nanofibrillated cellulose, Biomacromolecules. 14 (2013) 503–511. doi:10.1021/bm301755u.

[22] L.N. Acquaroli, P. Newby, C. Santato, Y.A. Peter, Thermal properties of methyltrimethoxysilane aerogel thin films, AIP Adv. 6 (2016) 105007–7. doi:10.1063/1.4965921.

[23] T. Kovacs, V. Naish, B. O'Connor, C. Blaise, F. Gagné, L. Hall, V. Trudeau, P. Martel, An ecotoxicological characterization of nanocrystalline cellulose (NCC), Nanotoxicology. 4 (2010) 255–270. doi:10.3109/17435391003628713.

[24] S. Wang, X. Peng, L. Zhong, J. Tan, S. Jing, X. Cao, W. Chen, C. Liu, R. Sun, An ultralight, elastic, cost-effective, and highly recyclable superabsorbent from microfibrillated cellulose fibers for oil spillage cleanup, J. Mater. Chem. A. 3 (2015) 8772–8781. doi:10.1039/c4ta07057g.

[25] H. Soeta, S. Fujisawa, T. Saito, L. Berglund, A. Isogai, Low-Birefringent and Highly Tough Nanocellulose-Reinforced Cellulose Triacetate, ACS Appl. Mater. Interfaces. 7 (2015) 11041–11046. doi:10.1021/acsami.5b02863.

[26] A. Baidya, M.A. Ganayee, S. Jakka Ravindran, K.C. Tam, S.K. Das, R.H.A. Ras, T. Pradeep, Organic Solvent-Free Fabrication of Durable and Multifunctional Superhydrophobic Paper from Waterborne Fluorinated Cellulose Nanofiber Building Blocks, ACS Nano. 11 (2017) 11091–11099. doi:10.1021/acsnano.7b05170.

[27] S. Zhao, Z. Zhang, G. Sèbe, R. Wu, R. V. Rivera Virtudazo, P. Tingaut, M.M. Koebel, Multiscale assembly of superinsulating silica aerogels within silylated nanocellulosic scaffolds: Improved mechanical properties promoted by nanoscale chemical compatibilization, Adv. Funct. Mater. 25 (2015) 2326–2334. doi:10.1002/adfm.201404368.

[28] B. Braun, J.R. Dorgan, Single-step method for the isolation and surface

functionalization of cellulosic nanowhiskers, Biomacromolecules. 10 (2009) 334–341. doi:10.1021/bm8011117.

[29] K. Missoum, J. Bras, M.N. Belgacem, Water redispersible dried nanofibrillated cellulose by adding sodium chloride, Biomacromolecules. 13 (2012) 4118–4125. doi:10.1021/bm301378n.

[30] M. Bentchikou, A. Guidoum, K. Scrivener, K. Silhadi, S. Hanini, Effect of recycled cellulose fibres on the properties of lightweight cement composite matrix, Constr. Build. Mater. 34 (2012) 451–456. doi:10.1016/j.conbuildmat.2012.02.097.

[31] T. Zhai, Q. Zheng, Z. Cai, L.S. Turng, H. Xia, S. Gong, Poly(vinyl alcohol)/cellulose nanofibril hybrid aerogels with an aligned microtubular porous structure and their composites with polydimethylsiloxane, ACS Appl. Mater. Interfaces. 7 (2015) 7436–7444. doi:10.1021/acsami.5b01679.

[32] J.R. McKee, S. Hietala, J. Seitsonen, J. Laine, E. Kontturi, O. Ikkala, Thermoresponsive nanocellulose hydrogels with tunable mechanical properties, ACS Macro Lett. 3 (2014) 266–270. doi:10.1021/mz400596g.

[33] A. Benchabane, K. Bekkour, Rheological properties of carboxymethyl cellulose (CMC) solutions, Colloid Polym. Sci. 286 (2008) 1173–1180. doi:10.1007/s00396-008-1882-2.

[34] T. ISHIKAWA, B. MUKAI, S. SHIRAISHI, N. UTOGUCHI, M. FUJI, M. MATSUMOTO, Y. WATANABE, Preparation of Rapidly Disintegrating Tablet Using New Types of Microcrystalline Cellulose (PH-M Series) and Low Substituted-Hydroxypropylcellulose or Spherical Sugar Granules by Direct Compression Method., Chem. Pharm. Bull. (Tokyo). 49 (2001) 134–139. doi:10.1248/cpb.49.134.

[35] K. Dutta, B. Das, J.T. Orasugh, D. Mondal, A. Adhikari, D. Rana, R. Banerjee, R. Mishra, S. Kar, D. Chattopadhyay, Bio-derived cellulose nanofibril reinforced poly(N-isopropylacrylamide)-g-guar gum nanocomposite: An avant-garde biomaterial as a transdermal membrane, Polymer (Guildf). 135 (2018) 85–102. doi:10.1016/j.polymer.2017.12.015.

[36] Z. Zhang, G. Sèbe, D. Rentsch, T. Zimmermann, P. Tingaut, Ultralightweight and flexible silylated nanocellulose sponges for the selective removal of oil from water,

Chem. Mater. 26 (2014) 2659–2668. doi:10.1021/cm5004164.

[37] S. Camarero Espinosa, T. Kuhnt, E.J. Foster, C. Weder, Isolation of thermally stable cellulose nanocrystals by phosphoric acid hydrolysis, Biomacromolecules. 14 (2013) 1223–1230. doi:10.1021/bm400219u.

[38] B. Wicklein, A. Kocjan, G. Salazar-Alvarez, F. Carosio, G. Camino, M. Antonietti, L. Bergström, Thermally insulating and fire-retardant lightweight anisotropic foams based on nanocellulose and graphene oxide, Nat. Nanotechnol. 10 (2015) 277–283. doi:10.1038/nnano.2014.248.

[39] A. Liu, L.A. Berglund, Fire-retardant and ductile clay nanopaper biocomposites based on montmorrilonite in matrix of cellulose nanofibers and carboxymethyl cellulose, Eur. Polym. J. 49 (2013) 940–949. doi:10.1016/j.eurpolymj.2012.12.017.

[40] F. Carosio, F. Cuttica, L. Medina, L.A. Berglund, Clay nanopaper as multifunctional brick and mortar fire protection coating-Wood case study, Mater. Des. 93 (2016) 357–363. doi:10.1016/j.matdes.2015.12.140.

[41] D.M. Fox, J. Lee, M. Zammarano, D. Katsoulis, D. V. Eldred, L.M. Haverhals, P.C. Trulove, H.C. De Long, J.W. Gilman, Char-forming behavior of nanofibrillated cellulose treated with glycidyl phenyl POSS, Carbohydr. Polym. 88 (2012) 847–858. doi:10.1016/j.carbpol.2012.01.015.

[42] Z. Zhang, P. Tingaut, D. Rentsch, T. Zimmermann, G. Sèbe, Controlled Silylation of Nanofibrillated Cellulose in Water: Reinforcement of a Model Polydimethylsiloxane Network, ChemSusChem. 8 (2015) 2681–2690. doi:10.1002/cssc.201500525.

[43] H. Sai, R. Fu, L. Xing, J. Xiang, Z. Li, F. Li, T. Zhang, Surface modification of bacterial cellulose aerogels' web-like skeleton for oil/water separation, ACS Appl. Mater. Interfaces. 7 (2015) 7373–7381. doi:10.1021/acsami.5b00846.

[44] B. Liu, L. Zhang, H. Wang, Z. Bian, Preparation of MCC/MC Silica Sponge and Its Oil/Water Separation Apparatus Application, Ind. Eng. Chem. Res. 56 (2017) 5795–5801. doi:10.1021/acs.iecr.6b04854.

[45] P.M. Dietrich, S. Glamsch, C. Ehlert, A. Lippitz, N. Kulak, W.E.S. Unger, Synchrotron-radiation XPS analysis of ultra-thin silane films: Specifying the organic silicon, Appl. Surf. Sci. 363 (2016) 406–411.

doi:10.1016/j.apsusc.2015.12.052.

[46] T. Fisher, M. Hajaligol, B. Waymack, D. Kellogg, Pyrolysis behavior and kinetics of biomass derived materials, J. Anal. Appl. Pyrolysis. 62 (2002) 331–349. doi:10.1016/s0165-2370(01)00129-2.

[47] I. Milosavljevic, V. Oja, E.M. Suuberg, Thermal effects in cellulose pyrolysis: Relationship to char formation processes, Ind. Eng. Chem. Res. 35 (1996) 653–662. doi:10.1021/ie950438l.

[48] V. Kokol, M. Božič, R. Vogrinčič, A.P. Mathew, Characterisation and properties of homo- and heterogenously phosphorylated nanocellulose, Carbohydr. Polym. 125 (2015) 301–313. doi:10.1016/j.carbpol.2015.02.056.

[49] S. Gaan, P. Rupper, V. Salimova, M. Heuberger, S. Rabe, F. Vogel, Thermal decomposition and burning behavior of cellulose treated with ethyl ester phosphoramidates: Effect of alkyl substituent on nitrogen atom, Polym. Degrad. Stab. 94 (2009) 1125–1134. doi:10.1016/j.polymdegradstab.2009.03.017.

[50] M.R. Alexander, R.D. Short, F.R. Jones, W. Michaeli, C.J. Blomfield, A study of HMDSO/O 2 plasma deposits using a high-sensitivity and -energy resolution XPS instrument: Curve fitting of the Si 2p core level, Appl. Surf. Sci. 137 (1999) 179–183. doi:10.1016/S0169-4332(98)00479-6.

[51] R. Gómez-Rojo, L. Alameda, Á. Rodríguez, V. Calderón, S. Gutiérrez-González, Characterization of Polyurethane Foam Waste for Reuse in Eco-Efficient Building Materials, Polymers (Basel). 11 (2019) 359. doi:10.3390/polym11020359.

[52] J. Hyuk Park, K. Suh Minn, H. Rae Lee, S. Hyun Yang, C. Bin Yu, S. Yeol Pak, C. Sung Oh, Y. Seok Song, Y. June Kang, J. Ryoun Youn, Cell openness manipulation of low density polyurethane foam for efficient sound absorption, J. Sound Vib. 406 (2017) 224–236. doi:10.1016/j.jsv.2017.06.021.

[53] X. Liu, J. Sun, S. Zhang, J. Guo, W. Tang, H. Li, X. Gu, Effects of carboxymethyl chitosan microencapsulated melamine polyphosphate on the flame retardancy and water resistance of thermoplastic polyurethane, Polym. Degrad. Stab. 160 (2019) 168–176. doi:10.1016/j.polymdegradstab.2018.12.019.

[54] Y.J. Chen, C.M. Shu, S.P. Ho, H.C. Kung, S.W. Chien, H.H. Ho, W.S. Hsu, Analysis of smoke movement in the Hsuehshan tunnel fire, Tunn. Undergr. Sp.

Technol. 84 (2019) 142–150. doi:10.1016/j.tust.2018.11.007.

[55] G. Shan, L. Jia, T. Zhao, C. Jin, R. Liu, Y. Xiao, A novel DDPSi-FR flame retardant treatment and its effects on the properties of wool fabrics, Fibers Polym. 18 (2017) 2196–2203. doi:10.1007/s12221-017-7244-2.

[56] M. Tokumura, S. Ogo, K. Kume, K. Muramatsu, Q. Wang, Y. Miyake, T. Amagai, M. Makino, Comparison of rates of direct and indirect migration of phosphorus flame retardants from flame-retardant-treated polyester curtains to indoor dust, Ecotoxicol. Environ. Saf. 169 (2019) 464–469. doi:10.1016/j.ecoenv.2018.11.052.

[57] M. Ba, B. Liang, C. Wang, Synthesis and characterization of a novel charring agent and its application in intumescent flame retardant polyethylene system, Fibers Polym. 18 (2017) 907–914. doi:10.1007/s12221-017-6899-z.

[58] A. Šehić, J. Vasiljević, I. Jordanov, A. Demšar, J. Medved, I. Jerman, M. Čolović, F. Hewitt, T.R. Hull, B. Simončič, Influence of N-, P- and Si-based Flame Retardant Mixtures on Flammability, Thermal Behavior and Mechanical Properties of PA6 Composite Fibers, Fibers Polym. 19 (2018) 1194–1206. doi:10.1007/s12221-018-8059-5.

[59] W. Guo, Y. Hu, X. Wang, P. Zhang, L. Song, W. Xing, Exceptional flame-retardant cellulosic foams modified with phosphorus-hybridized graphene nanosheets, Cellulose. 26 (2019) 1247–1260. doi:10.1007/s10570-018-2127-2.

[60] J.J. Cheng, W.J. Qu, S.H. Sun, Mechanical properties improvement and fire hazard reduction of expandable graphite microencapsulated in rigid polyurethane foams, Polym. Compos. 40 (2019) E1006–E1014. doi:10.1002/pc.24786.

[61] D. Xu, K. Yu, K. Qian, Effect of tris(1-chloro-2-propyl)phosphate and modified aramid fiber on cellular structure, thermal stability and flammability of rigid polyurethane foams, Polym. Degrad. Stab. 144 (2017) 207–220. doi:10.1016/j.polymdegradstab.2017.08.019.

[62] J. Guo, G. Liu, Y. Guo, L. Tian, X. Bao, X. Zhang, B. Yang, J. Cui, Enhanced flame retardancy and smoke suppression of polypropylene by incorporating zinc oxide nanowires, J. Polym. Res. 26 (2019). doi:10.1007/s10965-018-1680-6.

[63] N.T. Cervin, L. Andersson, J.B.S. Ng, P. Olin, L. Bergström, L. Waìšgberg, Lightweight and strong cellulose materials made from aqueous foams stabilized

by nanofibrillated cellulose, Biomacromolecules. 14 (2013) 503–511. doi:10.1021/bm301755u.

[64] M. Obori, D. Suh, S. Yamasaki, T. Kodama, T. Saito, A. Isogai, J. Shiomi, Parametric Model to Analyze the Components of the Thermal Conductivity of a Cellulose-Nanofibril Aerogel, Phys. Rev. Appl. 11 (2019) 1. doi:10.1103/PhysRevApplied.11.024044.

[65] T. Jayaramudu, H.U. Ko, H.C. Kim, J.W. Kim, E.S. Choi, J. Kim, Adhesion properties of poly(ethylene oxide)-lignin blend for nanocellulose composites, Compos. Part B Eng. 156 (2019) 43–50. doi:10.1016/j.compositesb.2018.08.063.

[66] H. Kim, J.R. Youn, Y.S. Song, Eco-friendly flame retardant nanocrystalline cellulose prepared via silylation, Nanotechnology. 29 (2018). doi:10.1088/1361-6528/aadc87.

[67] J.M. Silva, H.S. Barud, A.B. Meneguin, V.R.L. Constantino, S.J.L. Ribeiro, Inorganic-organic bio-nanocomposite films based on Laponite and Cellulose Nanofibers (CNF), Appl. Clay Sci. 168 (2019) 428–435. doi:10.1016/j.clay.2018.12.003.

[68] M. Santiago-Calvo, V. Blasco, C. Ruiz, R. París, F. Villafañe, M.Á. Rodríguez-Pérez, Improvement of thermal and mechanical properties by control of formulations in rigid polyurethane foams from polyols functionalized with graphene oxide, J. Appl. Polym. Sci. 136 (2019) 1–10. doi:10.1002/app.47474.

[69] S. Alasti Bonab, J. Moghaddas, M. Rezaei, In-situ synthesis of silica aerogel/polyurethane inorganic-organic hybrid nanocomposite foams: Characterization, cell microstructure and mechanical properties, Polymer (Guildf). 172 (2019) 27–40. doi:10.1016/j.polymer.2019.03.050.

[70] S. Wang, S. Xue, C. Ge, Q. Ren, D. Zhao, W. Zhai, Preparation of fluorescent thermoplastic polyurethane microcellular foam films blown by supercritical CO 2, J. Cell. Plast. (2019) 0021955X1984105. doi:10.1177/0021955X19841053.

[71] X. Ji, D. Chen, J. Shen, S. Guo, Flexible and flame-retarding thermoplastic polyurethane-based electromagnetic interference shielding composites, Chem. Eng. J. 370 (2019) 1341–1349. doi:10.1016/j.cej.2019.03.293.

[72] Z.J. Cao, W. Liao, S.X. Wang, H.B. Zhao, Y.Z. Wang, Polyurethane foams with

functionalized graphene towards high fire-resistance, low smoke release, superior thermal insulation, Chem. Eng. J. 361 (2019) 1245–1254. doi:10.1016/j.cej.2018.12.176.

[73] Y. Chen, C. Weng, Z. Wang, T. Maertens, P. Fan, F. Chen, M. Zhong, J. Tan, J. Yang, Preparation of polymeric foams with bimodal cell size: An application of heterogeneous nucleation effect of nanofillers, J. Supercrit. Fluids. 147 (2019) 107–115. doi:10.1016/j.supflu.2019.02.015.

[74] S. Zhang, Z. Ren, S. He, Y. Zhu, C. Zhu, FTIR spectroscopic characterization of polyurethane-urea model hard segments (PUUMHS) based on three diamine chain extenders, Spectrochim. Acta - Part A Mol. Biomol. Spectrosc. 66 (2007) 188–193. doi:10.1016/j.saa.2006.02.041.

[75] L. Liao, X. Li, Y. Wang, H. Fu, Y. Li, Effects of surface structure and morphology of nanoclays on the properties of jatropha curcas oil-based waterborne polyurethane/ clay nanocomposites, Ind. Eng. Chem. Res. 55 (2016) 11689–11699. doi:10.1021/acs.iecr.6b02527.

[76] J. Lubczak, E. Chmiel, Polyurethane Foams with 1,3,5-Triazine Ring and Silicon Atoms, Macromol. Res. (2019) 543–550. doi:10.1007/s13233-019-7068-6.

[77] B. Zhao, D.Y. Liu, W.J. Liang, F. Li, J.S. Wang, Y.Q. Liu, Bi-phase flame-retardant actions of water-blown rigid polyurethane foam containing diethyl-N,N-bis(2-hydroxyethyl) phosphoramide and expandable graphite, J. Anal. Appl. Pyrolysis. 124 (2017) 247–255. doi:10.1016/j.jaap.2016.12.032.

[78] X. Chen, L. Huo, C. Jiao, S. Li, TG-FTIR characterization of volatile compounds from flame retardant polyurethane foams materials, J. Anal. Appl. Pyrolysis. 100 (2013) 186–191. doi:10.1016/j.jaap.2012.12.017.

[79] B. Zhao, S. Xu, M. Adeel, S. Zheng, Formation of POSS-POSS interactions in polyurethanes: From synthesis, morphologies to shape memory properties of materials, Polymer (Guildf). 160 (2019) 82–92. doi:10.1016/j.polymer.2018.11.026.

[80] C. Luo, J. Zuo, F. Wang, Y. Yuan, F. Lin, J. Zhao, Preparation and Properties of Halogen-Free Flame Retardant and High Refractive Index Optical Resin via Click Chemistry, Macromol. Res. 26 (2018) 346–352. doi:10.1007/s13233-018-6045-8.

[81] X. Liu, J. Guo, W. Tang, H. Li, X. Gu, J. Sun, S. Zhang, Enhancing the flame retardancy of thermoplastic polyurethane by introducing montmorillonite nanosheets modified with phosphorylated chitosan, Compos. Part A Appl. Sci. Manuf. 119 (2019) 291–298. doi:10.1016/j.compositesa.2019.02.009.

[82] W. Xi, L. Qian, L. Li, Flame Retardant Behavior of Ternary Synergistic Systems in Rigid Polyurethane Foams, Polymers (Basel). 11 (2019) 207. doi:10.3390/polym11020207.

[83] X. Liu, S. Qin, H. Li, J. Sun, X. Gu, S. Zhang, J.C. Grunlan, Combination Intumescent and Kaolin-Filled Multilayer Nanocoatings that Reduce Polyurethane Flammability, Macromol. Mater. Eng. 304 (2019) 1–7. doi:10.1002/mame.201800531.

[84] H. Ding, K. Huang, S. Li, L. Xu, J. Xia, M. Li, Flame retardancy and thermal degradation of halogen-free flame-retardant biobased polyurethane composites based on ammonium polyphosphate and aluminium hypophosphite, Polym. Test. 62 (2017) 325–334. doi:10.1016/j.polymertesting.2017.07.017.

[85] S.D. Shaw, A. Blum, R. Weber, K. Kannan, D. Rich, D. Lucas, C.P. Koshland, D. Dobraca, S. Hanson, L.S. Birnbaum, Halogenated flame retardants: Do the fire safety benefits justify the risks?, Rev. Environ. Health. 25 (2010) 261–305. doi:10.1515/REVEH.2010.25.4.261.

[86] Y. Wu, C. Yao, Y. Hu, S. Yang, Y. Qing, Q. Wu, Flame retardancy and thermal degradation behavior of red gum wood treated with hydrate magnesium chloride, J. Ind. Eng. Chem. 20 (2014) 3536–3542. doi:10.1016/j.jiec.2013.12.046.

[87] K. Wu, Y. Hu, H.L.L. Song, Z. Wang, Flame retardancy and thermal degradation of intumescent flame retardant starch-based biodegradable composites, Ind. Eng. Chem. Res. 48 (2009) 3150–3157. doi:10.1021/ie801230h.

[88] X. Wang, L. Song, H. Yang, H. Lu, Y. Hu, Synergistic effect of graphene on antidripping and fire resistance of intumescent flame retardant poly(butylene succinate) composites, Ind. Eng. Chem. Res. 50 (2011) 5376–5383. doi:10.1021/ie102566y.

[89] T.H. Nguyen, D.Q. Hoang, J. Kim, Effect of ammonium polyphosphate and melamine pyrophosphate on fire behavior and thermal stability of unsaturated

polyester synthesized from poly(ethylene terephthalate) waste, Macromol. Res. 26 (2018) 22–28. doi:10.1007/s13233-018-6004-5.

[90] G. Huang, J. Yang, X. Wang, J. Gao, Nanoclay, intumescent flame retardants, and their combination with chemical modification for the improvement of the flame retardant properties of polymer nanocomposites, Macromol. Res. 21 (2013) 27–34. doi:10.1007/s13233-012-0185-0.

[91] S. Li, C. Li, C. Li, M. Yan, Y. Wu, J. Cao, S. He, Fabrication of nano-crystalline cellulose with phosphoric acid and its full application in a modified polyurethane foam, Polym. Degrad. Stab. 98 (2013) 1940–1944. doi:10.1016/j.polymdegradstab.2013.06.017.

[92] M.K. Chang, S.S. Hwang, S.P. Liu, Flame retardancy and thermal stability of ethylene-vinyl acetate copolymer nanocomposites with alumina trihydrate and montmorillonite, J. Ind. Eng. Chem. 20 (2014) 1596–1601. doi:10.1016/j.jiec.2013.08.004.

[93] S. Vecchiato, L. Skopek, S. Jankova, A. Pellis, W. Ipsmiller, A. Aldrian, B. Mueller, E. Herrero Acero, G.M. Guebitz, Enzymatic Recycling of High-Value Phosphor Flame-Retardant Pigment and Glucose from Rayon Fibers, ACS Sustain. Chem. Eng. 6 (2018) 2386–2394. doi:10.1021/acssuschemeng.7b03840.

[94] H.Q. Peng, Q. Zhou, D.Y. Wang, L. Chen, Y.Z. Wang, A novel charring agent containing caged bicyclic phosphate and its application in intumescent flame retardant polypropylene systems, J. Ind. Eng. Chem. 14 (2008) 589–595. doi:10.1016/j.jiec.2008.05.011.

[95] M. Jimenez, S. Duquesne, S. Bourbigot, Multiscale experimental approach for developing high-performance intumescent coatings, Ind. Eng. Chem. Res. 45 (2006) 4500–4508. doi:10.1021/ie060040x.

[96] Y. jin Chung, Y. Kim, S. Kim, Flame retardant properties of polyurethane produced by the addition of phosphorous containing polyurethane oligomers (II), J. Ind. Eng. Chem. 15 (2009) 888–893. doi:10.1016/j.jiec.2009.09.018.

[97] I. van der Veen, J. de Boer, Phosphorus flame retardants: properties, production, environmental occurrence, toxicity and analysis., Chemosphere. 88 (2012) 1119–53. doi:10.1016/j.chemosphere.2012.03.067.

[98] T.R. Hull, A. Witkowski, L. Hollingbery, Fire retardant action of mineral fillers, Polym. Degrad. Stab. 96 (2011) 1462–1469. doi:10.1016/j.polymdegradstab.2011.05.006.

[99] L. Kong, H. Guan, X. Wang, In Situ Polymerization of Furfuryl Alcohol with Ammonium Dihydrogen Phosphate in Poplar Wood for Improved Dimensional Stability and Flame Retardancy, ACS Sustain. Chem. Eng. 6 (2018) 3349–3357. doi:10.1021/acssuschemeng.7b03518.

[100] L.A. Hollingbery, T.R. Hull, The thermal decomposition of huntite and hydromagnesite-A review, Thermochim. Acta. 509 (2010) 1–11. doi:10.1016/j.tca.2010.06.012.

[101] L. Qian, Y. Qiu, J. Wang, W. Xi, High-performance flame retardancy by char-cage hindering and free radical quenching effects in epoxy thermosets, Polymer (Guildf). 68 (2015) 262–269. doi:10.1016/j.polymer.2015.05.031.

[102] Y.Q. Shi, T. Fu, Y.J. Xu, D.F. Li, X.L. Wang, Y.Z. Wang, Novel phosphorus-containing halogen-free ionic liquid toward fire safety epoxy resin with well-balanced comprehensive performance, Chem. Eng. J. 354 (2018) 208–219. doi:10.1016/j.cej.2018.08.023.

[103] J. Zhao, Q. Zhao, C. Wang, B. Guo, C.B. Park, G. Wang, High thermal insulation and compressive strength polypropylene foams fabricated by high-pressure foam injection molding and mold opening of nano-fibrillar composites, Mater. Des. 131 (2017) 1–11. doi:10.1016/j.matdes.2017.05.093.

[104] J. Park, S.H. Yang, K.S. Minn, C. Bin Yu, S.Y. Pak, Y.S. Song, J.R. Youn, Design and numerical analysis of syntactic hybrid foam for superior sound absorption, Mater. Des. 142 (2018) 212–220. doi:10.1016/j.matdes.2018.01.040.

[105] P.O. Darnerud, Toxic effects of brominated flame retardants in man and in wildlife, Environ. Int. 29 (2003) 841–853. doi:10.1016/S0160-4120(03)00107-7.

[106] J. Park, J.R. Youn, Y.S. Song, Carbon Nanotube Embedded Nanostructure for Biometrics, ACS Appl. Mater. Interfaces. 9 (2017) 44724–44731. doi:10.1021/acsami.7b15567.

[107] B. Wicklein, A. Kocjan, G. Salazar-Alvarez, F. Carosio, G. Camino, M. Antonietti, L. Bergström, Thermally insulating and fire-retardant lightweight anisotropic

foams based on nanocellulose and graphene oxide, Nat. Nanotechnol. 10 (2015) 277–283. doi:10.1038/nnano.2014.248.

[108] H. Kim, J.R. Youn, Y.S. Song, Eco-friendly flame retardant nanocrystalline cellulose prepared via silylation, Nanotechnology. (2018). doi:10.1088/1361-6528/aadc87.

[109] O. Köklükaya, F. Carosio, L. Wågberg, Superior Flame-Resistant Cellulose Nanofibril Aerogels Modified with Hybrid Layer-by-Layer Coatings, ACS Appl. Mater. Interfaces. 9 (2017) 29082–29092. doi:10.1021/acsami.7b08018.

[110] Y. Cheng, G. He, A. Barras, Y. Coffinier, S. Lu, W. Xu, S. Szunerits, R. Boukherroub, One-step immersion for fabrication of superhydrophobic/superoleophilic carbon felts with fire resistance: Fast separation and removal of oil from water, Chem. Eng. J. 331 (2018) 372–382. doi:10.1016/j.cej.2017.08.088.

[111] X. Qiu, Z. Li, X. Li, Z. Zhang, Flame retardant coatings prepared using layer by layer assembly: A review, Chem. Eng. J. 334 (2018) 108–122. doi:10.1016/j.cej.2017.09.194.

[112] J.H. Park, S.H. Yang, H.R. Lee, C. Bin Yu, S.Y. Pak, C.S. Oh, Y.J. Kang, J.R. Youn, Optimization of low frequency sound absorption by cell size control and multiscale poroacoustics modeling, J. Sound Vib. 397 (2017) 17–30. doi:10.1016/j.jsv.2017.03.004.

[113] L. Jiao, H. Xiao, Q. Wang, J. Sun, Thermal degradation characteristics of rigid polyurethane foam and the volatile products analysis with TG-FTIR-MS, Polym. Degrad. Stab. 98 (2013) 2687–2696. doi:10.1016/j.polymdegradstab.2013.09.032.

[114] D. Wee, D.G. Seong, J.R. Youn, Processing of microcellular nanocomposite foams by using a supercritical fluid, Fibers Polym. 5 (2004) 160–169. doi:10.1007/BF02902932.

[115] M.S. Koo, K. Chung, J.R. Youn, Reaction injection molding of polyurethane foam for improved thermal insulation, Polym. Eng. Sci. 41 (2001) 1177–1186. doi:10.1002/pen.10819.

[116] C. Kim, J.R. Youn, Environmentally friendly processing of polyurethane foam for thermal insulation, Polym. - Plast. Technol. Eng. 39 (2000) 163–185.

doi:10.1081/PPT-100100022.

[117] M. Floros, L. Hojabri, E. Abraham, J. Jose, S. Thomas, L. Pothan, A.L. Leao, S. Narine, Enhancement of thermal stability, strength and extensibility of lipid-based polyurethanes with cellulose-based nanofibers, Polym. Degrad. Stab. 97 (2012) 1970–1978. doi:10.1016/j.polymdegradstab.2012.02.016.

[118] S.T. McKenna, T.R. Hull, The fire toxicity of polyurethane foams, Fire Sci. Rev. 5 (2016) 3. doi:10.1186/s40038-016-0012-3.

[119] X. Liu, K.A. Salmeia, D. Rentsch, J. Hao, S. Gaan, Thermal decomposition and flammability of rigid PU foams containing some DOPO derivatives and other phosphorus compounds, J. Anal. Appl. Pyrolysis. 124 (2017) 219–229. doi:10.1016/j.jaap.2017.02.003.

Korean Abstract

초 록

본 논문에서는 나노셀룰로오스를 이용하여 난연 특성을 가지는 멤브레인과 발포 폴리우레탄에 관한 연구를 수행하였다. 나노크리스탈라인 셀룰로오스를 화학적으로 개질하여 실란화를 달성 하였으며, 셀룰로오스와 실란화에 이용한 물질은 가연성을 보이나, 이를 통해 생성되는 폴리실록세인이 표면에 막을 형성하여 난연성을 증가시킴을 확인하였다. 이러한 셀룰로오스를 이용하여 한계산소농도(LOI)가 매우 높고, 열전도도가 낮은 셀룰로오스를 멤브레인 형태로 제조하였다. 또한 피브릴화된 셀룰로오스와 상용 난연제를 동시에 폴리우레탄 폼에 첨가하여 시너지 효과를 유발시켜, 열방출속도, 연기발생속도 등이 낮고, 한계산소농도가 탁월한 발포 폴리우레탄 복합재료를 제조하였다. 특히, 실란화된 나노셀룰로오스가 발포를 위한 핵으로 작용하여 난연제의 단점인 셀 크기가 증가하는 문제를 해결함으로써 평균 셀 크기를 감소시킴과 동시에 발포가 저하되는 현상을 억제함을 확인하였다. 이러한 발포 고분자 복합재료는 기존의 폴리우레탄 폼보다 더 좋은 난연성을 가짐은 물론 친환경적인 충진제를 사용하였기 때문에, 인체에 유해한 상용 난연제의 사용을 감소시키는 효과를 제시하였다.

주요어: 고분자 재료, 나노셀룰로오스, 실란화, 실란화된 나노셀룰로오스, 난연성, 난연성 재료, 폴리우레탄폼, 고분자 복합재료, 복합재료 폼.

학 번: 2014-30203